CHAPTER 10: EVAPORATION COOLING CONCEPT, EVOLVE

Contributors

Lead Author: Rich Mattas
S. Malang
H. Khater
S. Majumdar
E. Mogahed
B. Nelson
M. Sawan
D.K. Sze

10. EVAPORATION COOLING CONCEPT, EVOLVE

10.1. Introduction, motivation for selecting the concept

Economically attractive fusion power plants require high power density, high thermal efficiency, and high availability in order to compensate for the high capital costs. First wall (FW) and breeding blankets are key components of such plants and their performance has a large impact on the attractiveness of the entire plant.

The APEX (Advanced Power Extraction)-study with the goal to explore the limits of FW/blanket-technology is based on the assumption that FW/blankets limit the allowable power density and not the divertors or the plasma itself. Really high limits for neutron wall load (>10 MW/m2), surface heat flux (>2 MW/m2), and thermal efficiency of the power conversion system (> 40%) have been set in this study for an initial screening of concepts to be included. The main reason for setting such a high scale is to "force" the invention of new concepts rather than to optimize already existing ones. On the other hand, it has been suggested not to exclude concepts at the beginning which do not meet all criteria for low activation materials in order to explore the high power density, high temperature regime.

The approach of the APEX-study is to assess concepts with thick liquid walls made of a breeder material (lithium, lithium alloys, or lithium containing molten salts) exposed directly to the plasma in order to reduce decisively activation and neutron damages of structural materials. There are some interesting ideas about such concepts but extensive work will be required to develop them to a point where the feasibility can be judged. Another possibility to avoid the frequent replacement of FW/blankets is to use a curtain made of solid breeder particles falling through the plasma chamber from the top to the bottom region, exposed directly to the plasma and extracting in this way the heat and the tritium generated by the neutrons. Again, this concept is not sufficiently mature to assess its feasibility.

Two other concepts included in the study are based on the use of solid FW's. One of them employs helium cooling of FW and breeding zone. A key feature of this concept is a structural material allowing a maximum temperature of ~1400 C in order to minimize the required heat transfer and, as a consequence of this, the pumping power.

The other concept named EVOLVE (Evaporation Of Lithium and Vapor Extraction) utilizes the exceptional high heat of evaporation of lithium (about 10 times higher than water) to remove the entire heat deposited in the first wall and blanket. A reasonable range of boiling temperatures of this alkali metal is 1200 to 1400 C, corresponding with a saturation pressure of 0.035 to ??? MPa. Such high temperatures make the use of refractory metals i.e. Mo, Ta, or W as structural material mandatory. These metals have sufficient strength and compatibility with lithium at these temperatures. For the FW they are required in any case for the given surface heat flux (>2 MW/m2)

because they are characterized by a high thermal conductivity (W : 100 W/(m* K)) . This heat flux would cause a high temperature gradient in a wall made of steel or vanadium resulting in excessive thermal stresses.

Heat transport by an evaporating liquid metal is employed in heat pipes too and there is considerable experience available with the system lithium/tungsten. For such a heat pipe a world record with 200 MW/m2 surface heat flux had been claimed, limited by the sonic velocity of the vapor. Capillary forces are employed in heat pipes to pump the liquid metal back to the evaporation site. This is probably not feasible for the geometry and the magnetic field in FW/blanket. Therefore EVOLVE is based on active pumping of the liquid metal, both in the first wall and the breeding region. The required liquid metal velocities are so low, that no insulating coatings are required to overcome MHD problems, and the pumping power will be negligibly small.

Different principles for heat extraction are used in first wall and breeding zone, all based on evaporation cooling with lithium at the same boiling temperature. The backside of the first wall is hit by an array of jets that maintain this surface wetted under all conditions. This liquid film is at boiling temperature and the heat is removed by the vapor generation. In the breeding zone the lithium is contained in flat trays. The reaction of the neutrons with Li causes volume heating and boiling of the stagnant liquid metal. All the heat deposited in the breeding zone is extracted by the vapor flow.

The combined vapor flow from first wall and breeding zone is condensed in a heat exchanger with helium flowing on the secondary side. This high temperature heat allows for the use of a closed cycle helium gas turbine power conversion system with a thermal efficiency up to 60 %.

The work on the EVOLVE concept is at a very early stage. Neither real design nor results of detailed analyses are available at this time. The purpose of this interim report is to provide the information's required for a first screening of the APEX concepts in order to identify concepts for further development. The following section contains descriptions of first wall, breeding zone, shielding, primary cooling loop, and power conversion system. First results of the analyses in the field of neutronics, thermal-hydraulics, tritium extraction, and safety are described in separate sections.

10.2. Design description

'The APEX FW/blanket concepts are based on a modified ARIES-RS Tokamak geometry. The same overall dimensions and the same replacement scheme (sector replacement through individual horizontal ports) is used for the EVOLVE concept. However, a single divertor at the bottom side replaces the double null divertors and the FW/blanket/shield is divided into upper and lower halves in order to reduce size and flow path length of the coolant manifolds. Figure 10.2-1 shows a vertical cross section of the torus and the maintenance port. In the EVOLVE concept, first wall and primary breeding zone are combined into one unit. Behind this unit, there is as a separate

component a high temperature shield at the inboard region and a secondary breeding blanket at the outboard region. Behind the secondary breeding zone there is , as a separate component too, an additional high temperature shield, required in order to meet the shielding requirements of vacuum vessel and magnets.

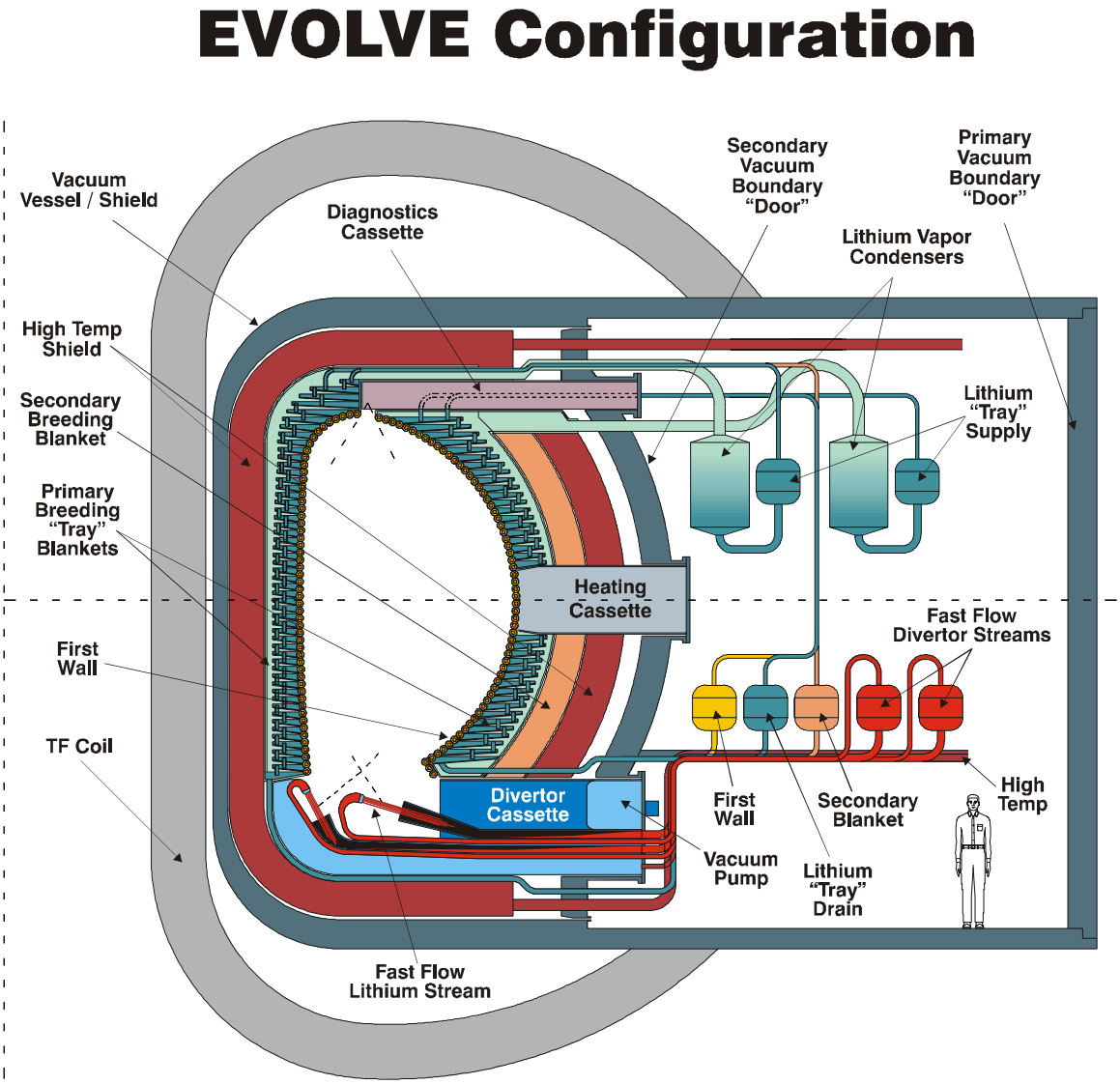

Figure 10.2-1. Cross-sectional view of the EVOLVE first wall/blanket concept

The same coolant (lithium) and structural material is used in all FW/breeding zones/ shields. Reference structural material is tungsten or a tungsten rhenium-alloy. An alternative material is a tantalum alloy, which is more ductile and workable than tungsten. Tungsten has, however, considerably higher thermal conductivity, higher strength at operating temperature, and better compatibility with lithium. An additional advantage of tungsten is the higher breeding rate achievable with this structural material. A combination of the two materials can also be considered where the large elements of the structure are fabricated of W and some connection elements made of Ta in order to combine the better neutronics feature and the lower cost of W with the higher ductility

and better weldability of Ta. Tungsten carbide is used as efficient shielding material. Novel ideas are employed for the first wall and the primary breeding zone and these concepts will be described in some detail. The secondary breeding zone is a self-cooled blanket with lithium as breeder and coolant. These components as well as the high temperature shields are more or less "standard" designs that have not been detailed in this study.

10.2.1 First Wall

The basic design of the concept is shown in fig.10.2-2. The FW is composed of U-shaped tubes, running in radial-toroidal-radial direction. Inside these tubes there are smaller feed tubes with an array of nozzles for the generation of liquid metal jets hitting the backside of the FW. The diameter of this feed tube has a maximum at the entrance and goes to zero at the exit, giving there the entire space to the vapor flow. There is some overlay of the footprint of the jets on the FW, providing some redundancy in case some of the jets fail. Simple small-bore tubes can be uses as nozzles, with typical dimensions in the order of 1 mm i.d. and 10 mm length. They act as MHD throttles, allowing to adjust the flow rate easily to the position. The jets are directed only to the front halve of the vapor tubes in order to remove there the large surface heat flux by evaporation. The volumetric heat generation in the second half of the tube is removed by heat conduction in azimuthal direction and by vapor convection cooling. Uniformity of heat removal from the first wall is an issue to be addressed in the future.

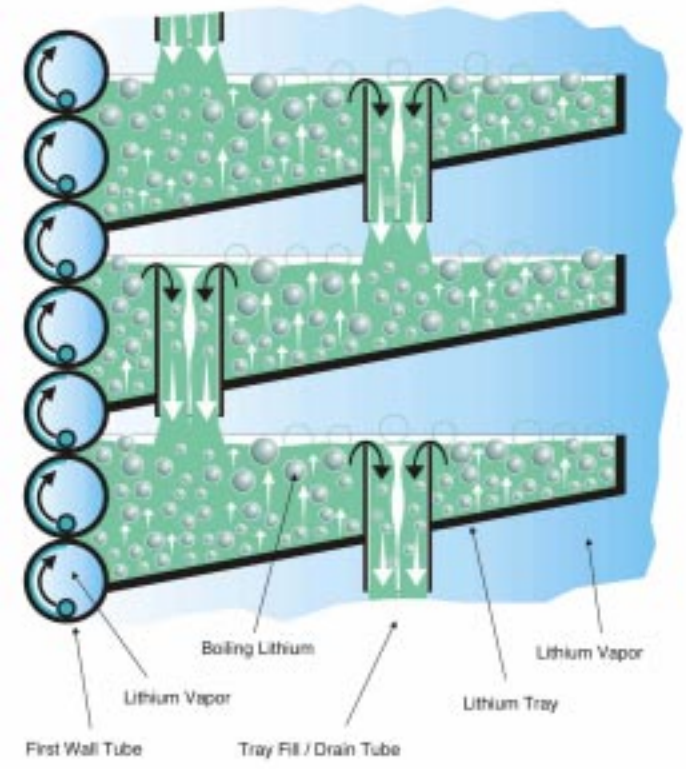

Figure 10.2-2. Schematic of EVLOVE first wall tubes and blanket trays containing Lithium

Given the large heat flux into the first wall, its thickness has to be kept to a minimum in order to minimize temperature differences and thermal stresses. This is facilitated by the low vapor pressure and a circular tube geometry, allowing a wall thickness of less than 3 mm. Typical dimensions for the vapor tubes and the feed tubes are inner diameters of 50 mm and 10 mm respectively.

For a surface heat flux of 2 MW/m2, a toroidal segment width of 3 m, and the tube dimensions given above, a boiling temperature of 1200 C (saturation pressure 0.035 MPa) results in a liquid metal velocity in the feed tube of about I m/s and a vapor velocity of about 500 m/s. This is about 1/3 of the sonic velocity and results in a tolerable pressure drop. The wall thickness of the feed tube can be made small enough to avoid excessive large MHD pressure drop without the need for insulating coatings. It is suggested to "overfeed" the FW by about 50 % to avoid any dryout. This means that the vapor at the exit of the tube will have entrained some liquid metal that will be separated in the manifold. In the present EVOLVE concept, there are combined vapor manifolds for first wall and primary breeding zone.

10.2.2 Primary breeding zone

Using of lithium evaporation cooling in the breeding zone in combination with the FW cooling described above offers a number of advantages

- Only one coolant required,
- Required liquid metal flow rate about a factor of ten lower than in a self-cooled lithium blanket,
- High heat transfer typical for boiling liquid metals result in exceptionally low temperature variation in the blanket, and as a consequence of this, in minimized thermal stresses.
- Low vapor pressure (reference value 0.035 MPa) leads to very low primary stresses.
- High vapor temperature allows for high efficiency power conversion system.

The main challenges for this concept are the difficult fabrication of the blanket structure with a tungsten alloy, an operating temperature of more than 1200 C, and the separation of the vapor from the stagnant liquid metal.

The principal design of the breeding zone can be seen in fig. 10.2-3. Flat trays are used as lithium containers in order to facilitate the vapor separation. Each tray contains a lithium pool with a height of 10 to 20 cm, which is maintained constant by a system of overflow tubes. The large volume heating of the lithium leads to rather violent boiling. The vapor bubbles have to rise in the pool and separate from the liquid metal at the surface. From here the vapor flows a short distance in parallel to the surface before it enters the vertical vapor manifold. Entrained liquid metal will be separated there.

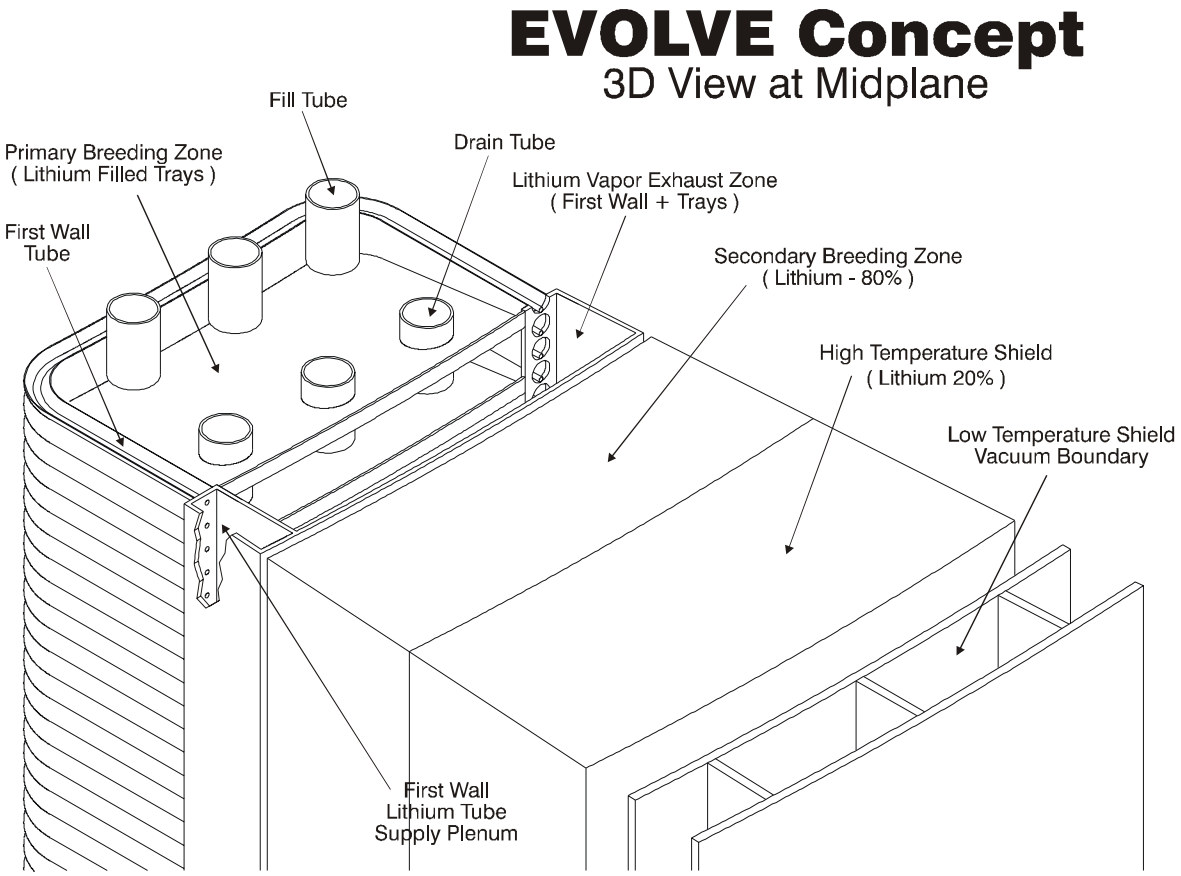

Fig. 10.2-3. Breeding zone design

The principle of the overflow system for maintaining constant lithium levels in all trays is shown in fig. 10.2-2. There is a fill pipe at the top of the stack and a drain pipe at the bottom of it. There will be always excess flow at the top in order to assure that all trays are full. This means that at the bottom continuously draining of a fraction of the total flow rate is required.

The trays with a thickness of about 5 mm are fabricated from flat sheets. They are attached to the FW, which is composed of a tube bank. The concept requires neither high precision in the fabrication nor high quality welds. Even large leaks between tray and FW tubes can be tolerated. The poloidal distances between the trays has to be optimized with the goal to provide sufficient space for the vapor flow but to avoid excessive gaps for neutron streaming.

A flat plate with a thickness of about 10 mm is used to close the vapor manifold in radial direction. Stiffening plates connecting it in radial direction to the U-shaped FW box support this plate. During operation there is vacuum at the outside of the component and a vapor pressure of 0.035 MPa at the inside, resulting in exceptional low primary stresses. Due to the boiling heat transfer at the inside, the temperature of the structure

will be close to the boiling temperature of the lithium and the total temperature variation will be very small, resulting in low thermal stresses.

10.2.3 Secondary breeding zone and high temperature shield

The total fraction of lithium in the primary breeding zone is rather low due to the gaps for vapor flow between trays, the vapor content in the lithium pools, and the low specific lithium density at boiling temperature. The resulting rather low tritium breeding ratio can be increased by increasing the 6Li enrichment, but there remains a need for arranging a secondary breeding zone in the outboard region where the space is not limited as much as in the inboard side. The neutron flux in the secondary breeding zone is considerably lower than at the front, allowing the use of a variety of blanket concepts. For simplicity reasons, however, a self-cooled lithium/tungsten blanket concept has been selected as reference solution in order to limit the number of materials used and to also allow the generation of high grade heat in this zone. The low volumetric heat generation and the absense of a surface heat flux probably enables a design without insulating coatings, where the MHD pressure drops are kept to a tolerable level by using thin-walled flow channel inserts. Neither design work nor analyses have been performed for this concept in the frame of this study, because self-cooled blanket concepts have been investigated in a number of blanket and power plant studies. The same statements can be applied to the high temperature shields required both at the inboard and the outboard region for additional neutron shielding of vacuum vessel and magnets. They are also made of tungsten as structural material, cooled by flowing lithium. Tungsten carbide is used as shielding material. Reasonable assumptions about the volume composition of these components have been made for the neutronics analysis.

10.2.4 Divertor

A preliminary design of the divertor for the EVOLVE concept has been developed and is shown in Fig. 10.2-4. The divertor cassette is similar to previous designs, but the collector plates have been replaced with flowing jets. The advantages of the jets include the ability to accommodate high surface heat loads, elimination of erosion concerns, and potential control of the plasma edge parameters. Free surface liquid divertors are presently being addressed by the Advanced Limiter-divertor Plasma-facing Systems (ALPS) program.

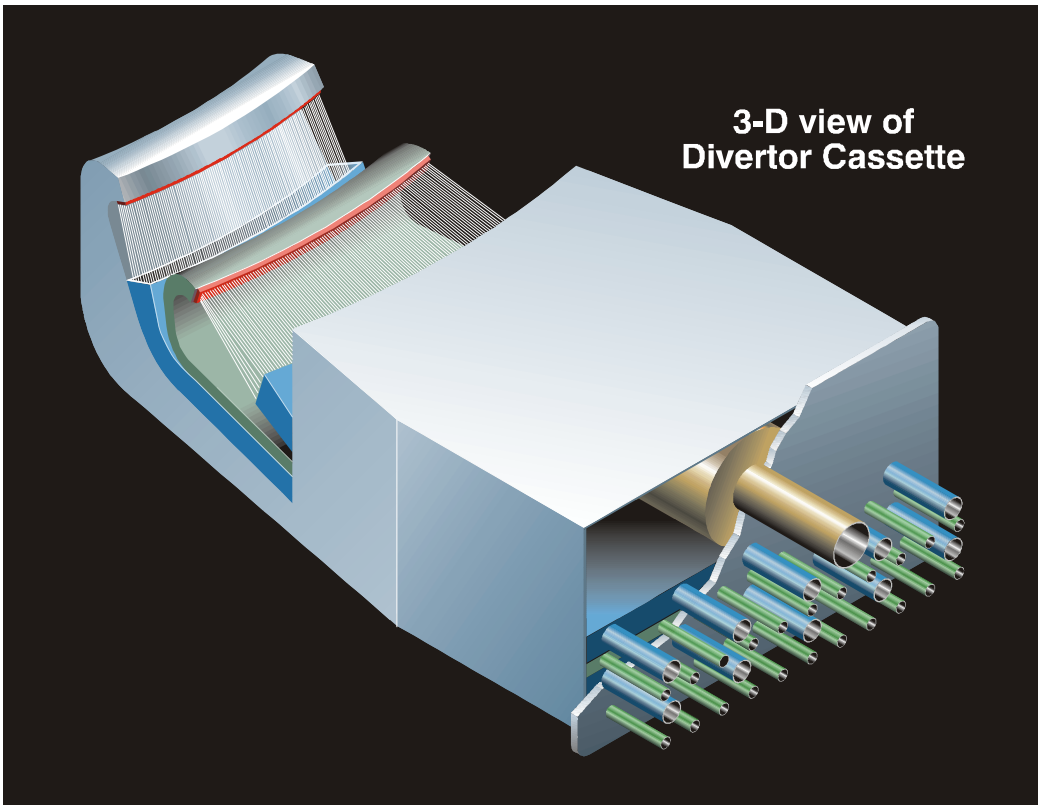

Fig. 10.2-4. Divertor cassette design

10.2.5 Primary cooling loops

Lithium is used as primary coolant for all components (FW, Primary breeding zone, secondary breeding zone, high temperature shield). About 2/3 of the total heat is extracted by lithium vapor at a temperature of 1200 C, the remaining 1/3 by the liquid metal cooling of the secondary breeding zone and the shields. The heat sink for both loops are the lithium/helium heat exchangers where the helium of the closed cycle gas turbine power conversion system is heated up to about 1000 C. In the evaporation loop the entire heat is transferred to the secondary helium by condensation. Due to the pressure drop in the vapor flow, vapor pressure and, as a consequence of this the saturation temperature will decrease. This means, that the liquid metal will exit from the IHX with a temperature of 900 to 1000 C. It is probably advantageous to pre-heat this liquid metal flow to about 1100 C with a small bypass flow of high temperature vapor before it enters the blanket in order to minimize thermal stresses.

The liquid metal temperatures in the convection cooled components can be chosen in a large range to optimize the power conversion system. The structure must be kept above 800 C in order to avoid embrittlement. The upper temperature limit is given by compatibility considerations which would allow for tungsten/lithium values up to 1400 C. A third limitation for the allowable temperature range is set by the temperature rise between coolant inlet and outlet. In general, large temperature rises should be

avoided in order to keep thermal stresses small. Altogether it may be advantageous to operate the convection loop between 1100 C at the inlet and 1200 C at the outlet at about the same level as the evaporation loop in order to minimize differential thermal expansion. Heat transfer in the HX of the evaporation loop is at the primary side by condensation and therefore very effective. There is a large temperature difference available for heat transfer to the helium in the convection loops. Both features would minimize the heat transfer surface area in the HX.

The relatively small size of these HX enables a design where the entire lithium loops including the intermediate heat exchanger are located inside the horizontal maintenance ports. There is one port anticipated for each torus sector in order to speed up blanket replacement by exchanging the entire sector. This offers the possibility to design modular heat exchangers, two for every torus sector (upper and lower halves). The result of this is an advantage in regard to safety and availability.

Keeping the entire lithium inside the vacuum chamber minimizes the risk of chemical reaction between lithium with water, air, concrete or other gases. Malfunctions in the cooling system of one sector will not have an impact on the function of the other sectors and provides in this way functioning heat sinks for radiating the after heat from a failed sector.

The downtime for a blanket exchange, and as a consequence of this, the availability of the blanket system is increased by this design because no liquid metal coolant lines have to be cut and rewelded inside the plasma chamber during a blanket replacement. The argument that the relatively large number of HX has a negative impact on the failure rate is not valid because this failure rate is mainly determined by the number of heat exchanger tubes which is independent from the degree of modularization.

The arrangement of the IHX inside the vacuum vessel implies a risk of pressurization in case of a tube rupture. This risk has to be avoided by locating suitable rupture disks for a fast release of the accidental helium pressure.

Future effort is needed to quantify the geometry and volumes required for the heat transfer system.

10.2.6 Power Conversion System

A natural choice for the power conversion system is a closed cycle gas turbine system since the heat is extracted from first wall and blankets at temperatures above 1000 C. A thermal efficiency up to about 57 % is achievable in such a system with these high temperatures.

Additional advantages of this Brayton cycle compared to a Rankine steam turbine cycle are smaller problems with tritium permeation losses to the environment and the possibility to use heat exchanger materials not compatible with steam or

impurities in helium. Tritium permeation losses are minimized by the fact that the only connection to the environment is the low temperature HX at the heat rejection system and the inter-cooler between the different compression stages.

The impurity level in the helium can be maintained at very low values since there are no sources for ingress of oxygen, water vapor or other gases. This means that it is possible to remove impurities by hot trapping to very low concentrations prior to heating up the heat exchanger to operating temperatures. This would not help in a system with helium/steam HX where unavoidable micro leaks would always be a source for impurities.

10.3 Neutronics

Neutronics and shielding calculations have been performed for the EVOLVE concept. The calculations were carried out in two stages. One-dimensional scoping calculations were performed to optimize the blanket design in order to achieve attractive nuclear performance. These calculations were used also to determine the radial build required to provide adequate shielding for the vacuum vessel and magnet. These calculations were followed by two-dimensional calculations to evaluate the nuclear performance parameters for the reference design. Two-dimensional modeling was performed to properly account for the effects of streaming through the gaps for vapor flow between the trays.

10.3.1 One-Dimensional Scoping Analysis

10.3.1.1 Calculational Procedure

Fig. 10.3-1 shows the configuration of the EVOLVE blanket. The first wall (FW) is composed of a tube bank. The outer tube is 0.3 cm thick and has an inner diameter of 5 cm. The size of the 0.1 cm thick inner tube varies toroidally and an average inner diameter of 1 cm is used in the analysis. The trays wall is 0.5 cm thick and are made of a refractory alloy. Both tungsten and tantalum alloys were considered. Each tray contains a lithium pool with a height ranging from 18 cm at the front to 14 cm at the back. The radial thickness of the trays in the OB region is 50 cm while the thickness in the IB region is 40 cm. A vapor manifold back plate with a thickness of 1 cm is used.

One-dimensional calculations were performed at three poloidal locations. These include a section through the Li tray and inner FW tube, a section through the Li tray without inner FW tube, and a section between Li trays without inner FW tube. The radial builds used for these calculations are given in Figs. 10.3-2, -3, and –4. The results were coupled with the appropriate coverage fractions to estimate the overall nuclear parameters. Both the inboard (IB) and outboard (OB) regions were modeled simultaneously to account for the toroidal effects. The results were normalized to OB and IB wall loading of 10 and 7 MW/m^2, respectively. The Li density in trays and FW is taken to be 0.35 g/cm^3 based on the density at saturation temperature and assuming 17% average vapor fraction.

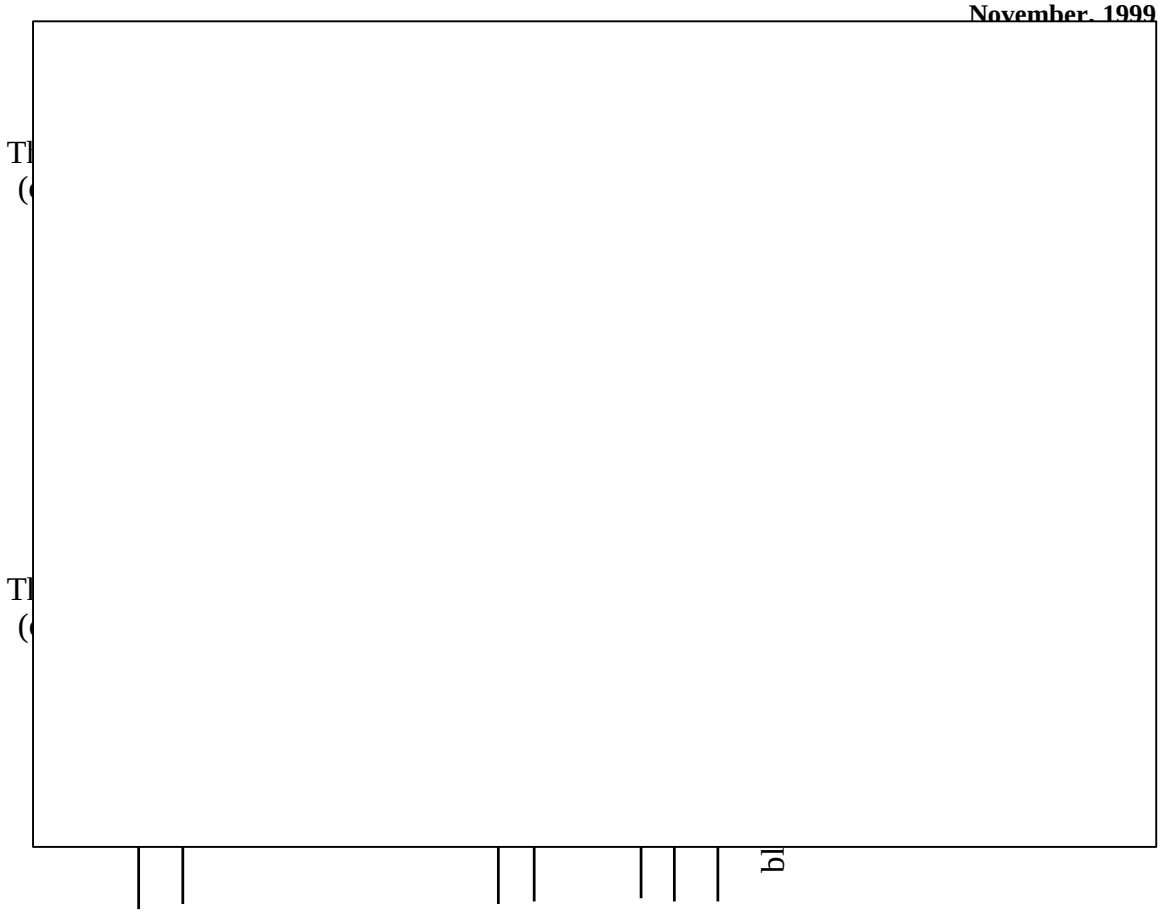

Fig. 10.3-3. Radial build for section through the Li tray without inner FW tube.

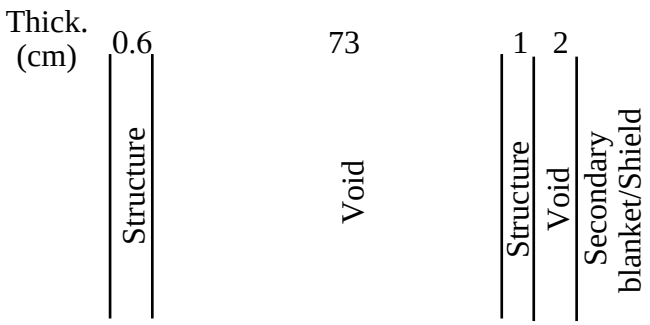

Fig. 10.3-4. Radial build for section between Li trays without inner FW tube.

10.3.1.2 Tritium Breeding

The local tritium breeding ratio (TBR) was determined in the OB and IB trays for the two candidate refractory alloys. Fig. 10.3-5 gives the variation with tray radial thickness when Ta alloy is used. For the same tray thickness, the IB local TBR is ~8% larger than the OB local TBR due to the toroidal geometrical effects. Fig. 10.3-6 compares the OB local TBR with W and Ta alloys. Using W alloy results in ~10% higher TBR compared to the case with Ta alloy and is used in the reference design. In addition, W is cheaper with better strength and compatibility while Ta has the edge in the area of fabrication and welding. The local TBR values for the trays were modified by the trays coverage fraction (72.7%) to determine the local OB and IB TBR values. To estimate the overall TBR, we assumed neutron coverage fractions of 75%, 15%, and 10% for the outboard, inboard, and divertor regions, respectively. The resulting overall TBR values are significantly below unity.

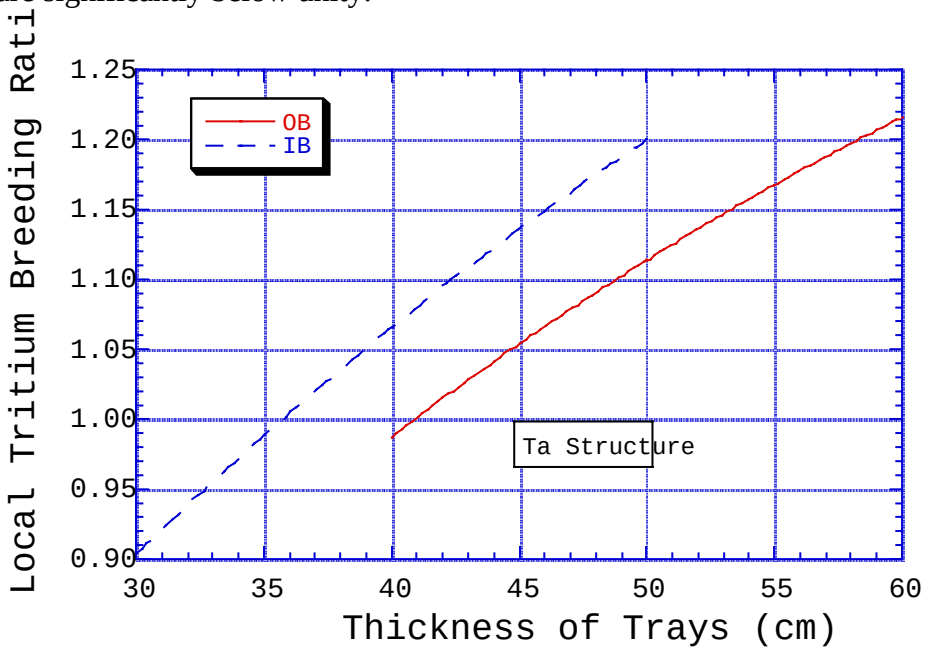

Fig. 10.3-5. Effect of tray radial thickness on local TBR with Ta structure.

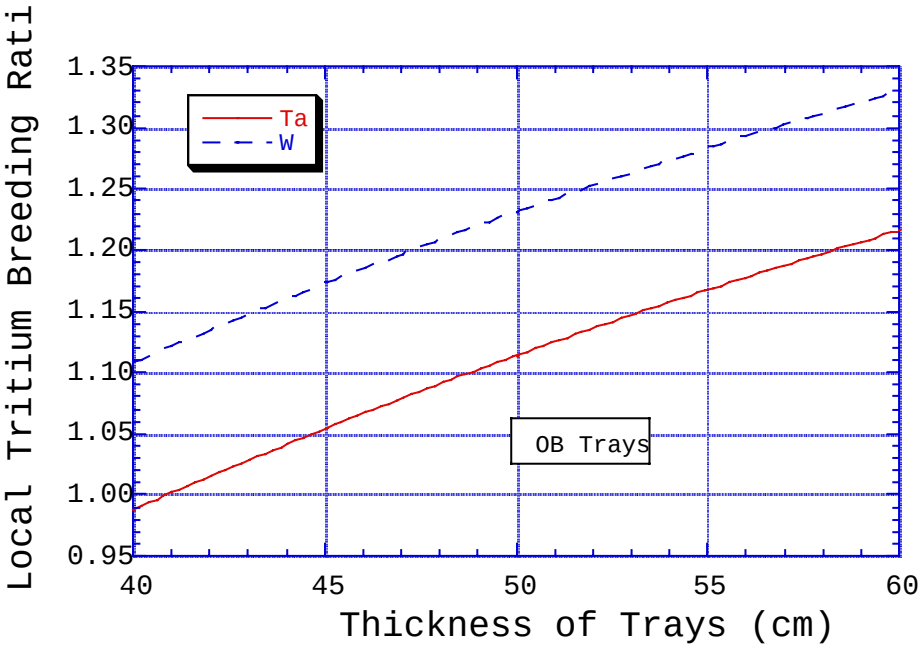

Fig. 10.3-6. Impact of structural material on local TBR.

A secondary breeding blanket is utilized to enhance the overall TBR. A 40-cm-thick secondary breeding blanket is employed in the OB side only where space is not constrained. The neutron flux in the secondary breeding zone is considerably lower than at the front, allowing the use of a variety of blanket concepts. For simplicity reasons, however, a self-cooled lithium/tungsten blanket concept has been selected as reference solution. Using W structure in the secondary blanket reduces the number of materials used and allows using high Li temperature for efficient power conversion. In addition, using W structure results is lower damage rate compared to steel (factors of ~3 lower dpa and ~50 lower He production). The secondary blanket was assumed to consist of 90% Li and 10% W. Both the IB and OB high temperature shields required for additional shielding of vacuum vessel (VV) and magnets are also made of tungsten as structural material and cooled by flowing lithium. Tungsten carbide is used as a shielding material. The composition of shield is considered to be 20% Li, 10% W, and 70% WC. Lithium at 0.53 g/cm^3 density is used in both the secondary blanket and shield.

The effect of enriching the lithium on the local TBR at different poloidal sections is illustrated in Fig. 10.3-7. Modest Li enrichment (30-50 % ^{6}Li) enhances the TBR. The TBR enhancement with enrichment is lower in the trays, with less structure, than in the secondary blanket and shield. Less than 1% of tritium breeding takes place in the FW. At sections through the trays, the secondary breeding blanket contributes ~25% of the local TBR in the OB region. The local TBR values were combined with coverage of trays (72.7%) and IB and OB coverage fractions to determine the estimated overall TBR. We made the conservative assumption of no breeding in the divertor region. Fig. 10.3-8 gives the overall TBR as a function of Li enrichment. The TBR maximizes at 40% ^{6}Li with a

value of 1.336. This is ~22% higher than the value for natural Li. Lithium enriched to 40% ^{6}Li is considered in the reference design. About 57% of the tritium breeding is contributed by the lithium in the trays. The secondary blanket and shield contribute 40% and 3% of the total tritium breeding, respectively. Tritium breeding has a comfortable margin that gives the flexibility to reduce the thickness of the breeding zones, allow for higher vapor content in the front zone, increase thickness of the structure, or include more shielding material in the secondary breeding blanket.

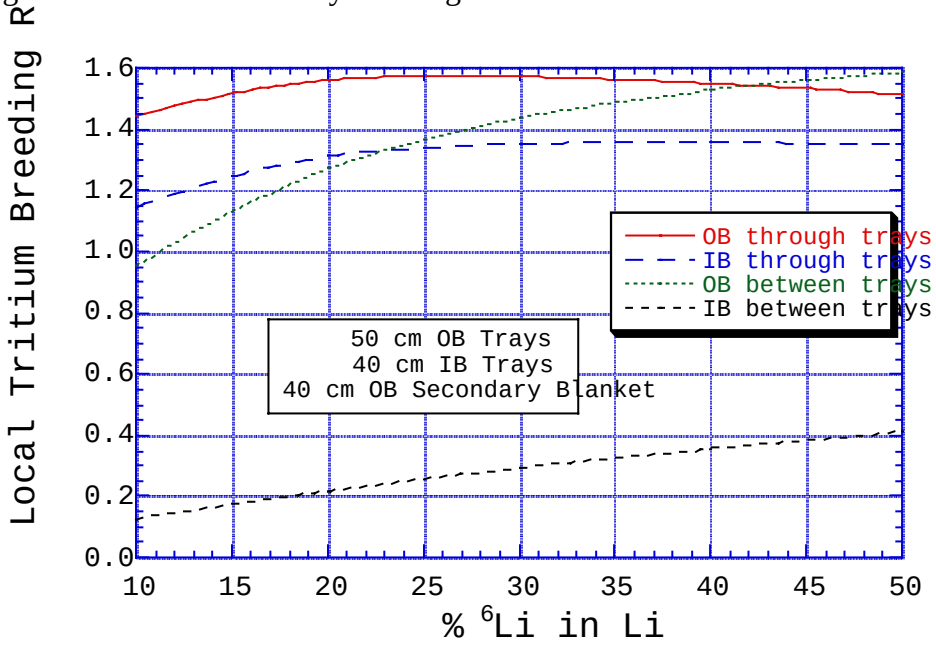

Fig. 10.3-7. Impact of Li enrichment on local TBR at different poloidal locations.

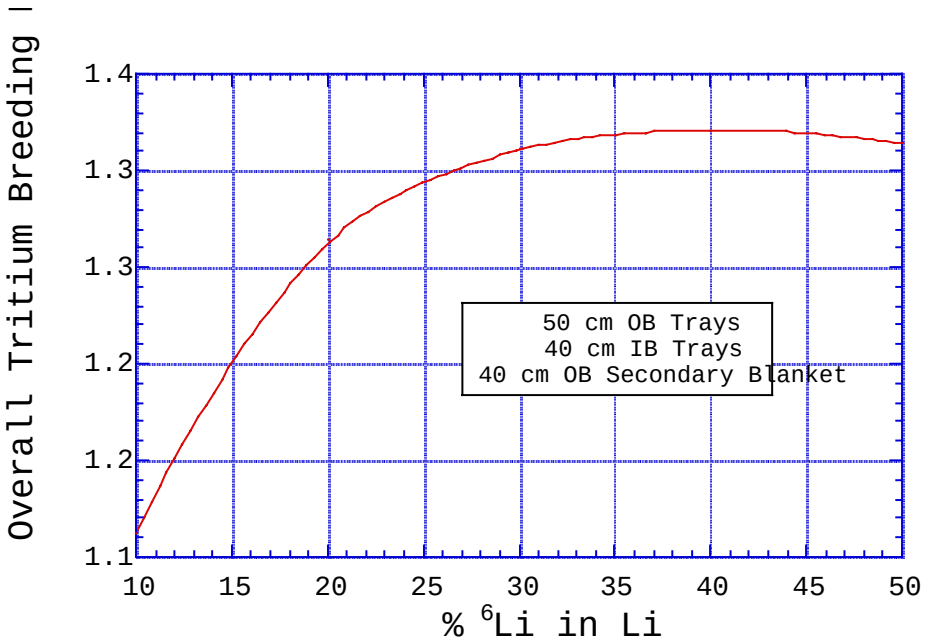

Fig. 10.3-8. Effect of Li enrichment on overall TBR.

10.3.1.3 Nuclear Heating

Nuclear heating in the blanket and shield components were calculated at locations through and between the trays. The results were coupled with the coverage of trays to determine the nuclear energy multiplication, M_n, defined as the amount of nuclear heating per unit neutron energy incident on the FW, in both the IB and OB regions. The values for the IB and OB regions are 1.145 and 1.216, respectively. Most of the nuclear heating (~60%) is deposited in the front blanket. Adding the surface heat deposited in the FW implies that ~66% of the total energy is deposited as high-grade heat in the front evaporation-cooled zone and carried to the heat exchanger by the Li vapor.

The peak W structure nuclear heating in the blanket and shield components has been calculated at locations through and between the trays. The results are given in Table 10.3-1. Peaking in FW nuclear heating occurs between the trays. The peaking factors are 1.3 in the OB region and 1.6 in the IB region. Nuclear heating peaking in the manifold backplate, secondary blanket, and shield resulting from streaming between the trays is a factor of ~3-5. The values between the trays are based on 1-D calculations and are very conservative estimates since the space between the FW and secondary blanket is assumed to be completely empty.

Table 10.3-1. Peak W nuclear heating (W/cm^3) based on 1-D calculations.

		IB	OB
Section Through Trays	FW	75.5	91.8
	Manifold Backplate	28.1	24.2
	Secondary Blanket	NA	21.5
	Shield	24.9	3.3
Section between Trays	FW	117.9	120.2
	Manifold Backplate	98.5	99.6
	Secondary Blanket	NA	85.3
	Shield	83	18.9

10.3.1.4 Structure Damage Rate

The peak dpa and helium production rates in the W structure have been determined at locations through and between trays. The results are given in Table 10.3-2. A slight peaking occurs in the FW damage between the trays. The peaking factors are 1.03 and 1.2 in the OB and IB regions, respectively. The peaking in the manifold backplate, secondary blanket, and shield resulting from streaming between the trays is a

factor of ~3-5 for dpa and ~8-11 for He production. Again, these are conservative estimates based on the 1-D calculations.

Table 10.3-2. Peak dpa rate (dpa/FPY) and He production rate (He appm/FPY) in W structure based on 1-D calculations.

		Dpa/FPY		He appm/FPY	
		IB	OB	IB	OB
Section Through Trays	FW	29.8	38.2	18.1	23.9
	Manifold Backplate	6.5	6.2	1.5	1.4
	Secondary Blanket	NA	5.5	NA	1.2
	Shield	5.5	0.64	1.2	0.07
Section between Trays	FW	35.6	39.2	21.3	24.6
	Manifold Backplate	25.2	29.2	12.7	15.8
	Secondary Blanket	NA	24.5	NA	12.2
	Shield	19.3	2.73	8.2	0.49

10.3.1.5 Shielding Requirements

The VV is located behind the shield. It consists of two steel sheets each 5 cm thick sandwitching a 30-cm-thick shielding zone made of 80% WC and 20% He. For the vacuum vessel to be reweldable, the cumulative helium production in the structure should not exceed 1 He appm. The shield thickness needed to reduce the peak helium production in the VV to less than 1 He appm after 30 FPY plant life was determined. The calculations were performed using the 1-D model for the section between the trays where VV damage is expected to be the highest. Fig. 10.3-9 shows the effect of shield thickness on the peak end-of-life helium production in the VV. The plant lifetime is assumed to be 30 full power years (FPY). Based on these results, the reference design uses a 50-cm-thick OB shield and a 60-cm-thick IB shield. Table 10.3-3 gives the peak neutronics parameters for the VV in both the inboard and outboard regions. The results clearly indicate that the VV is reweldable.

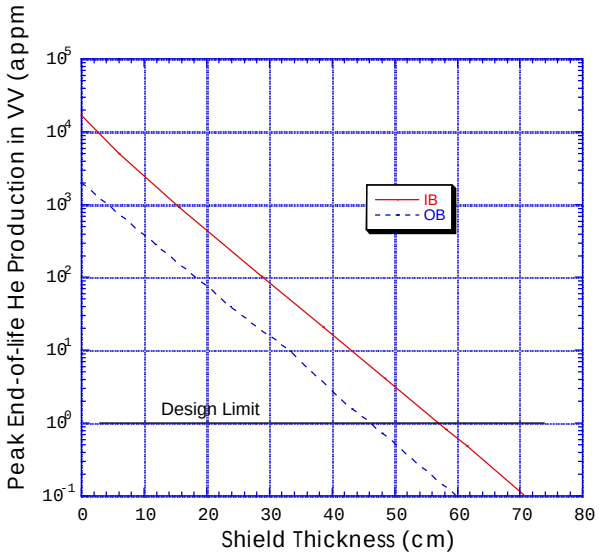

Fig.10.3-9. Effect of shield thickness on peak end-of-life helium production in the VV.

Table 10.3-3.. Peak VV neutronics parameters.

	IB	OB
Peak Nuclear Heating (mW/cm^3)	6.4	4.8
Peak end-of-life dpa	0.14	0.11
Peak end-of-life He appm	0.57	0.42

Adequate shielding must be provided for the superconducting magnets such that their performance is not degraded by neutron and gamma radiation. The component most sensitive to radiation is the organic insulator because of possible degradation in mechanical strength. Radiation damage could also affect the critical properties of the superconductor and the resistivity of the copper stabilizer. In addition magnet nuclear heating that is removed by cryogenic liquid helium should be limited. We will assume that the magnet radiation limits are similar to those adopted in the ITER design. These are end-of-life fast neutron fluence of 10^{19} n/cm^2, end-of-life dose to the insulator of 10^9 Rads, $6x10^{-3}$ end-of-life dpa to Cu stabilizer, and 1 mW/cm^3 peak nuclear heating. Table 10.3-4 gives the peak radiation effects in the magnet located behind the 40-cm-thick VV. It is clear that all magnet radiation limits are satisfied.

Table 10.3-4. Peak magnet neutronics parameters

	IB	OB	Design Limit
Peak Nuclear Heating (mW/cm^3)	0.033	0.022	1
Peak end-of-life Fast Neutron Fluence, E> 0.1 MeV (n/cm^2)	$7.5x10^{17}$	$5.0x10^{17}$	10^{19}
Peak end-of-life Dose to Epoxy Insulator (Rads)	$8.8x10^8$	$6.0x10^8$	10^9
Peak end-of-life dpa to Cu Stabilizer	$4x10^{-4}$	$2.7x10^{-4}$	$6x10^{-3}$

10.3.1.6 Recommended Radial Build for the Reference Design

The radial build that satisfies requirements for vacuum vessel reweldability, and superconductor magnet shielding was determined for both the IB and OB regions. The total IB radial build between the FW and magnet is 165.5 cm. In the OB region, the total radial build is 212.5 cm. Table 10.3-5 gives the breakdown of the radial build in both the IB and OB regions. Based on the 1-D scoping analysis, this configuration allows for tritium self-sufficiency with an estimated overall TBR of 1.34. In addition, it leads to about two thirds of the thermal power being carried by the high temperature Li vapor.

Table 10.3-5. Recommended radial build for the reference design.

	IB	OB
FW	5 cm	5 cm
Li tray	40 cm	50 cm
Back wall of tray	0.5 cm	0.5 cm
Li vapor manifold	15 cm	20 cm
Manifold backplate	1 cm	1 cm
Clearance	2 cm	2 cm
Secondary blanket	0 cm	40 cm
Clearance	0 cm	2 cm
Shield	60 cm	50 cm
Clearance	2 cm	2 cm
VV front sheet	5 cm	5 cm
VV shielding zone	30 cm	30 cm
VV rear sheet	5 cm	5 cm
Total	165.5 cm	212.5 cm

10.3.2 Two-Dimensional Neutronics Analysis for the Reference EVOLVE Design

10.3.2.1 Calculational Model

Two-dimensional (2-D) modeling of the front evaporation cooled blanket of EVOLVE is needed to properly account for the poloidal heterogeniety and gaps between trays. The nuclear heating and damage hot spots at the parts of the OB secondary blanket and IB shield between trays, estimated from the 1-D calculations, are conservatively high. The 1-D calculations assume the space between the FW and secondary blanket to be completely empty resulting in overestimating the streaming effects. The R-Z geometrical 2-D model used in the calculation is shown in Fig.10.3-10. It includes the FW, trays with Li vapor manifold, secondary breeding blanket, shield, VV, and magnet in both the IB and OB regions. Both the IB and OB regions are modeled simultaneously to account for the toroidal effects. Due to the limitations of 2-D modeling, the trays are assumed to have a uniform height of 16 cm. In addition, the detailed FW tube configuration is not modeled and the FW is represented by a 0.6 thick plate. These design details require 3-D modeling and are not expected to affect the neutronics results.

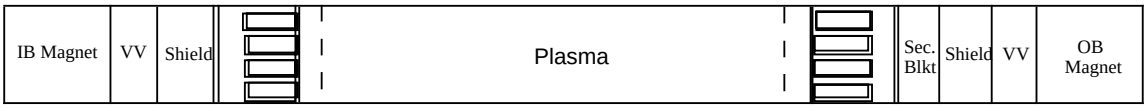

Fig. 10.3-10. R-Z two-dimensional model for EVOLVE.

The TWODANT module of the DANTSYS 3.0 discrete ordinates particle transport code system was utilized. An inherent problem associated with multi-dimensional discrete ordinates calculations is referred to as the “ray effect”. It is related

to the fact that the angular flux is given only in certain discrete directions which could lead to underestimating neutron streaming. This effect is mitigated by using the ray tracing first collision source option in TWODANT.

10.3.2.2 Tritium Breeding Ratio

The overall TBR calculated for the reference design using the 2-D model is 1.37 with Li-6 enrichment of 40%. It is based on the conservative assumption of no breeding in the divertor region. 69.8% of tritium breeding occurs in the trays (57.3% OB and 12.5% IB). The OB secondary blanket contributes 27.7% of the total overall TBR (20.2% behind trays and 7.5% between trays). The contribution of the shield is only 2.5% (1% OB and 1.5% IB). Tritium breeding has a comfortable margin that allows for design flexibility. The overall TBR determined from the 2-D calculation is slightly higher than that estimated from the 1-D calculations coupled with coverage fractions (1.37 vs. 1.336). The contribution to TBR from the trays is much larger than that estimated from the 1-D calculations (69.8% vs. 57%) due to the larger chance of intercepting the neutrons in the trays before reaching the secondary blanket and shield.

10.3.2.3 Nuclear Heating Distribution

Nuclear heating in the blanket and shield components was calculated using the 2-D model. The nuclear energy multiplication, M_n, defined as amount of nuclear heating per unit neutron energy incident on the FW, is given in Table 10.3-6 for both the IB and OB components. The nuclear heating in the FW and trays is ~20% higher than estimated from the 1-D calculations. Nuclear heating in the secondary breeding blanket and shield is ~30% lower than estimated from the 1-D results due to the larger chance of intercepting the neutrons in the trays before reaching the secondary blanket and shield. For a nominal fusion power of 1 GW, Fig. 10.3-11 shows the nuclear heating partitioning in the EVOLVE components. Most of the nuclear heating (~72%) is deposited in the evaporation cooled front blanket. Adding the surface heat deposited in the FW implies that ~76% of the total IB and OB energy is deposited as high grade heat in the front evaporation cooled zone (FW and trays) and carried by the Li vapor to the heat exchanger.

Table 10.3-6. Nuclear energy multiplication in IB and OB components.

	IB	OB
Front Blanket	0.883	0.856
Back Blanket	NA	0.304
Shield	0.310	0.041
Total	1.193	1.201

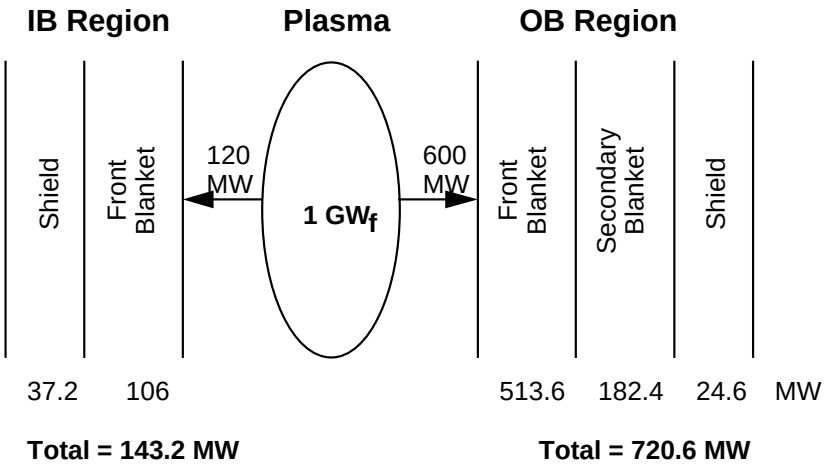

Fig. 10.3-11. Nuclear heating partitioning in the reference EVOLVE design.

The peak W structure nuclear heating in the blanket and shield components obtained from the 2-D calculation is given in Table 10.3-7. The peak heating in the manifold backplate, secondary blanket, and shield is a factor of 3-4 lower than predicted from the 1-D calculations. No significant poloidal peaking is observed in the nuclear heating profiles. Since the source is volumetrically distributed, most source neutrons are intercepted by the FW and trays. The secondary neutrons and gamma rays which give large contribution to nuclear heating tend to give nearly poloidally uniform profiles. Fig. 10.3-12 shows the radial variation of nuclear heating at the bottom of the OB trays. The results are given for the tray structure and the Li adjacent to it. At any radial location the power density in the W bottom of the tray is more than a factor of 3 higher than that in the Li adjacent to it.

Table 10.3-7. Peak structure nuclear heating (W/cm^3) in blanket and shield components

	IB	OB
FW	85.0	105.8
Manifold Backplate	33.3	31.3
Secondary Blanket	NA	26.2
Shield	20.1	4.3

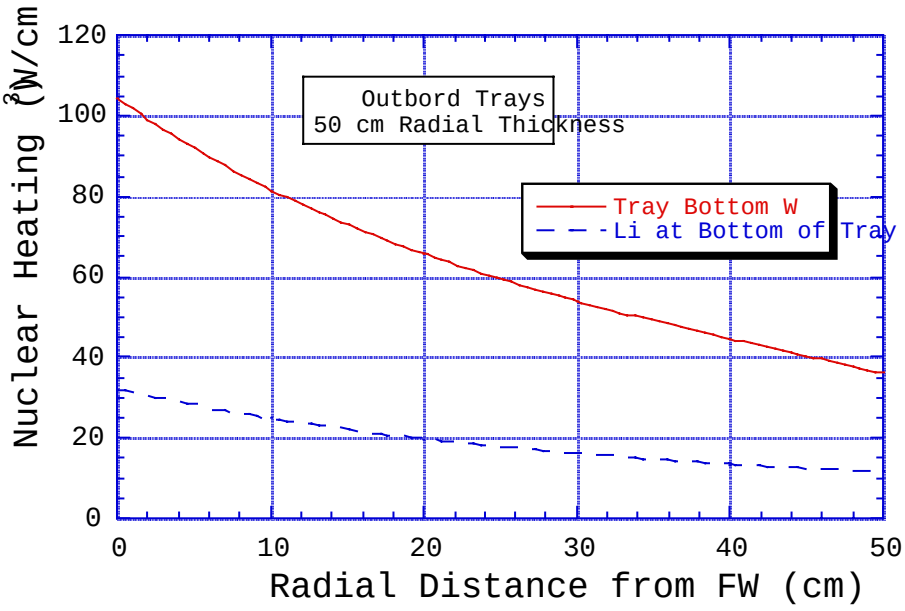

Fig.10.3-12. Nuclear heating at the bottom of the tray.

10.3.2.4 Radiation Damage in the Structural Material

The peak dpa and helium production rates have been determined in the W structure using the 2-D model. Table 10.3-8 gives the results. No significant poloidal peaking is observed. The peak dpa rate in the manifold backplate, secondary blanket, and shield is a factor of ~3-5 lower than predicted from the 1-D calculations while He production is a factor of ~6-10 lower. This confirms that the peaking from the 1-D calculations was very conservative. The peak damage rate in the OB secondary blanket and IB shield is about a factor of ~6 lower than in the FW and, hence, they are expected to have a factor of 6 longer lifetime than the FW and trays. The lifetime of the OB shield is about an order of magnitude longer than for the OB secondary blanket and the IB shield making it a lifetime component.

Table 10.3-8. Peak dpa and He production rates in the W structure.

	Dpa/FPY		He appm/FPY	
	IB	OB	IB	OB
FW	25.7	34.8	14.0	20.2
Manifold Backplate	7.0	7.0	2.0	2.0
Secondary Blanket	NA	6.1	NA	1.8
Shield	4.3	0.74	1.3	0.12

Neutron streaming through the gaps between trays results in the largest poloidal flux peaking at the back surface of the trays. This flux peaking decreases rapidly as one moves away from the trays towards the secondary blanket and shield as evidence from the results in Fig. 10.3-13. Fig. 10.3-14 shows the poloidal variation of the dpa rate around an OB tray. The results are given for the FW, the front surface of the secondary blanket, and the front surface of the shield. Slight damage peaking occurs in the FW in front of trays due to increased neutron reflection. Damage is nearly poloidally uniform in the secondary blanket and shield. Fig. 10.3-15 compares the 1-D and 2-D predictions for poloidal variation of damage rate at the front of the OB secondary blanket. It is clear that the 1-D calculations significantly overestimate the peak damage rate in the secondary blanket. The situation is similar for the OB shield as shown in Fig. 10.3-16. The radial variation of dpa and He production rates in the tray structure is given in Fig. 10.3-17. The dpa rate drops by a factor of 5 from the FW to the back of the tray. On the other hand, the He production rate drops by a factor of 9 from the FW to the back of the tray.

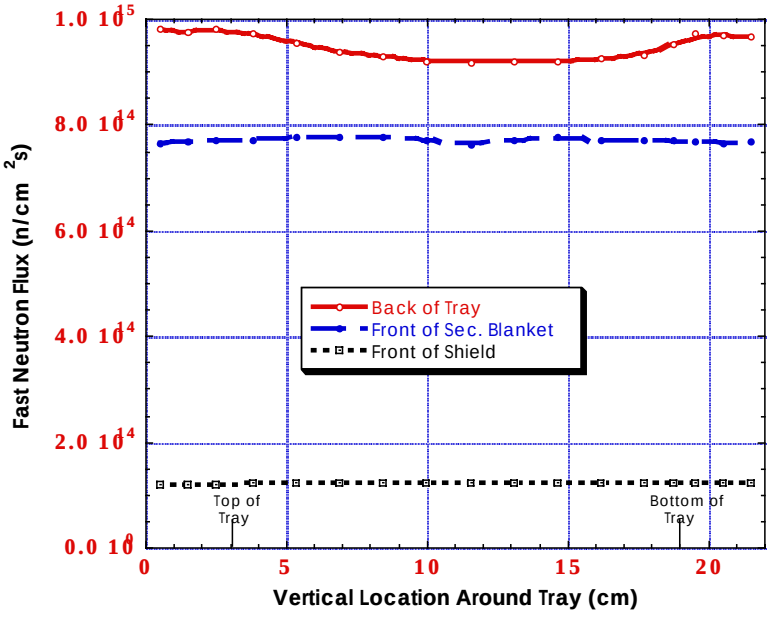

Fig. 10.3-13. Poloidal variation of fast neutron flux.

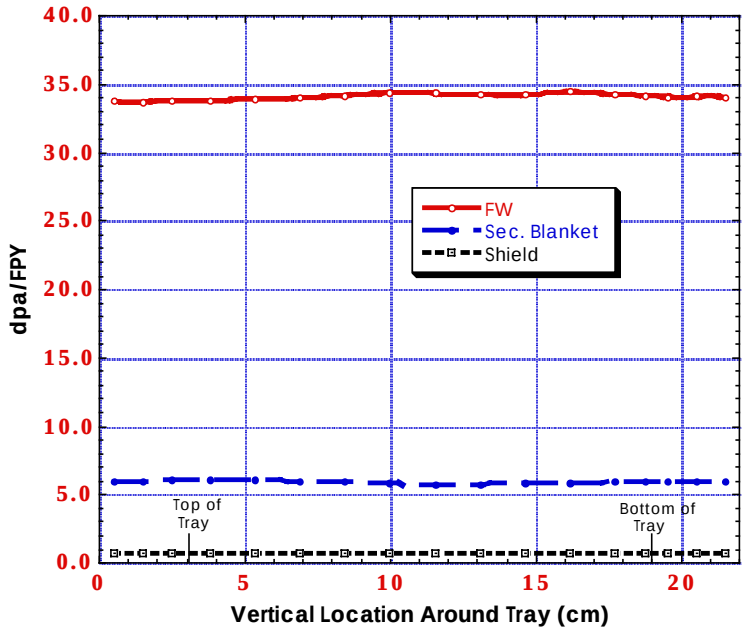

Fig. 10.3-14. Poloidal variation of damage rate around an OB tray.

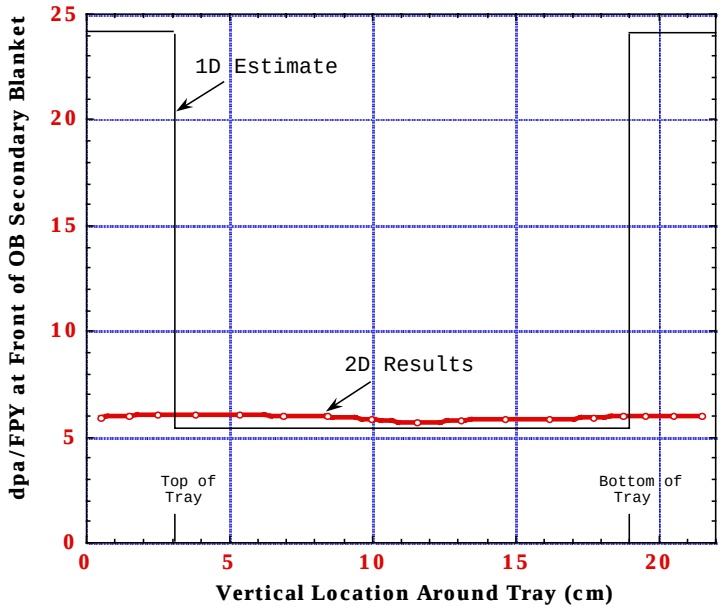

Fig. 10.3-15. Poloidal distribution of dpa rate at front of OB secondary blanket.

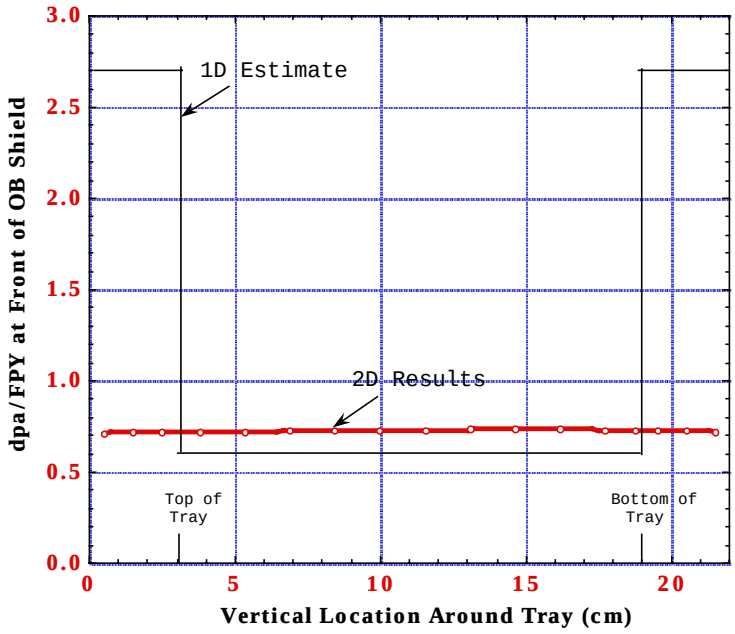

Fig. 10.3-16. Poloidal distribution of dpa rate at front of OB shield.

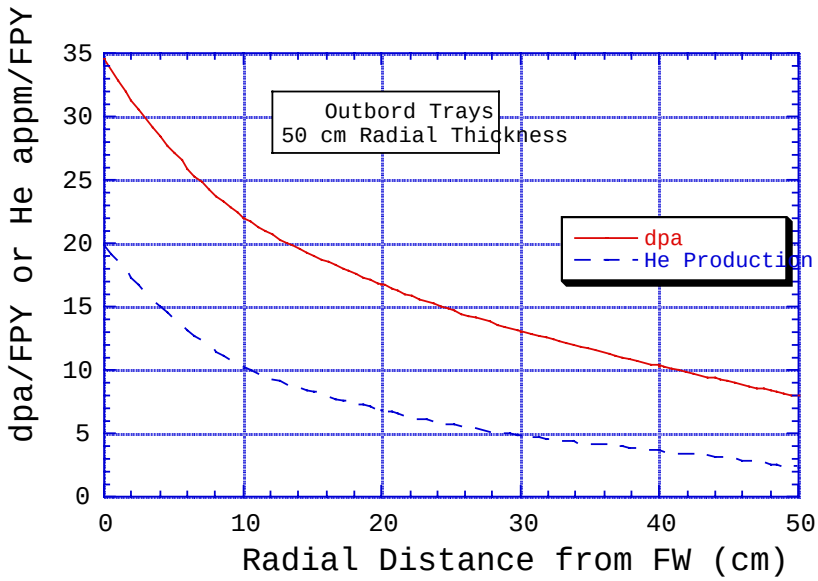

Fig. 10.3-17. Radial variation of dpa and He production rates in OB tray structure.

10.3.2.5 Peak Vacuum Vessel and Magnet Nuclear Parameters

Based on the 1-D scoping calculations, the radial build required for vacuum vessel reweldability, and superconductor magnet shielding was determined for both the IB and OB regions. This was used in the 2-D model. Table 10.3-9 gives the peak

neutronics parameters for the VV. The peak end-of-life He production in the VV is less than the 1 appm required for reweldability. In addition, all magnet radiation limits are satisfied as shown in Table 10.3-10.

Table 10.3-9. Peak VV neutronics parameters.

	IB	OB
Peak Nuclear Heating (mW/cm^3)	2.8	2.0
Peak end-of-life dpa	0.08	0.05
Peak end-of-life He appm	0.30	0.21

Table 10.3-10. Peak magnet neutronics parameters.

	IB	OB	Design Limit
Peak Nuclear Heating (mW/cm^3)	0.039	0.023	1
Peak end-of-life Fast Neutron Fluence (n/cm^2)	$8.4x10^{17}$	$5.4x10^{17}$	10^{19}
Peak end-of-life Dose to Epoxy Insulator (Rads)	$1.0x10^{9}$	$6.4x10^{8}$	10^{9}
Peak end-of-life dpa to Cu Stabilizer	$4.8x10^{-4}$	$2.7x10^{-4}$	$6x10^{-3}$

10.4. Activation Analysis

10.4.1 Introduction

Activation analysis was performed for the EVOLVE concept. Calculations are performed assuming neutron wall load of 7 and 10 MW/m^2 at the inboard and outboard first walls, respectively. The analysis used the W-5Re alloy as a structure material in the first wall and blanket. The elemental composition of the W-5Re alloy is shown in Table 10.4-I. In this section the term "first wall" refers to the first wall and tray as a single unit. The WC alloy was used as a shielding material. Based on dpa limits for tungsten, the inboard and outboard first walls were assumed to be replaced every 5 FPY. On the other hand, the outboard blanket, shield and vacuum vessel are assumed to stay in place for 30 FPY. Two-dimensional calculations are needed to take in to account the neutron streaming through the gaps between the trays. The 2-D model used in the calculation is shown in Fig. 10.3-1. Neutron transport calculations were performed using the discrete ordinates neutron transport code DANTSYS.

The neutron flux obtained from the neutron transport calculations was used in the activation calculations. The activation analysis was performed using the activation code DKR-PULSAR2.0. The code combined the neutron flux with the FENDL/A-2.0 data library to calculate the activity and decay heat as a function of time following shutdown. Calculated specific activities were used to calculate the waste disposal ratings (WDR) of the different components at the end of their life-time. Results of the decay heat analysis were used to evaluate the temperature variation exhibited by the structure during a loss of coolant accident (LOCA).

10.4.2 Activity and Decay Heat

Figures 10.4-1 and 10.4-2 show the specific activity and decay heat values induced in the different components as a function of time following shutdown, respectively. As shown in both figures, the W-5Re alloy produces high level of radioactivity after shutdown. The first wall and blanket dominate the overall activity and decay heat induced in the structure. Table 10.4-II shows a list of nuclides that dominate the induced radioactivity in the different components. As shown in the table, the tungsten isotopes $^{181}W(T_{1/2}$ = 121 day), $^{185}W(T_{1/2}$ = 75.1 day), and $^{184}Re(T_{1/2}$ = 38 day) are the main contributors to the induced radioactivity during the first few weeks following shutdown. Neutron interactions and subsequent decays of both tungsten and rhenium produce these isotopes. The long-term radioactivity is generated by the $^{179}Ta(T_{1/2}$ = 665 day), $^{182}Ta(T_{1/2}$ = 115 day), and $^{186m}Re(T_{1/2} = 2x10^5$ yr) isotopes. Out of these three isotopes, ^{186m}Re is the most troublesome because it is considered as a major contributor to the waste disposal ratings at the end of the plant life-time. In addition, ^{186m}Re is also one of the main contributors to the off-site doses during an accident.

Table 10.4-I. Elemental Composition of the W-5Re Alloy.

Nuclide	wt% or wppm
H	5 wppm
C	30 wppm
N	10 wppm
O	30 wppm
Na	10 wppm
Mg	5 wppm
Al	15 wppm
Si	20 wppm
P	50 wppm
S	5 wppm
K	10 wppm
Ca	10 wppm
Ti	10 wppm
Cr	10 wppm
Mn	5 wppm
Fe	30 wppm
Co	10 wppm
Ni	20 wppm
Cu	10 wppm
Zn	5 wppm
As	5 wppm
Zr	10 wppm

Nb	10 wppm
Mo	100 wppm
Ag	5 wppm
Cd	10 wppm
Ba	10 wppm
Ta	10 wppm
W	94.96%
Re	5 %
Pb	10 wppm

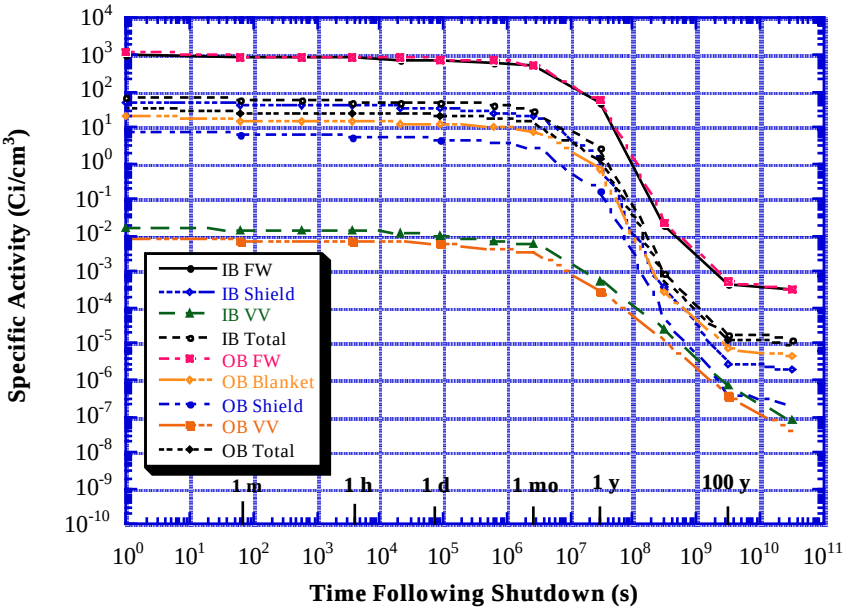

Fig. 10.4-1. Activity induced in the different components of EVOLVE as a function of time following shutdown.

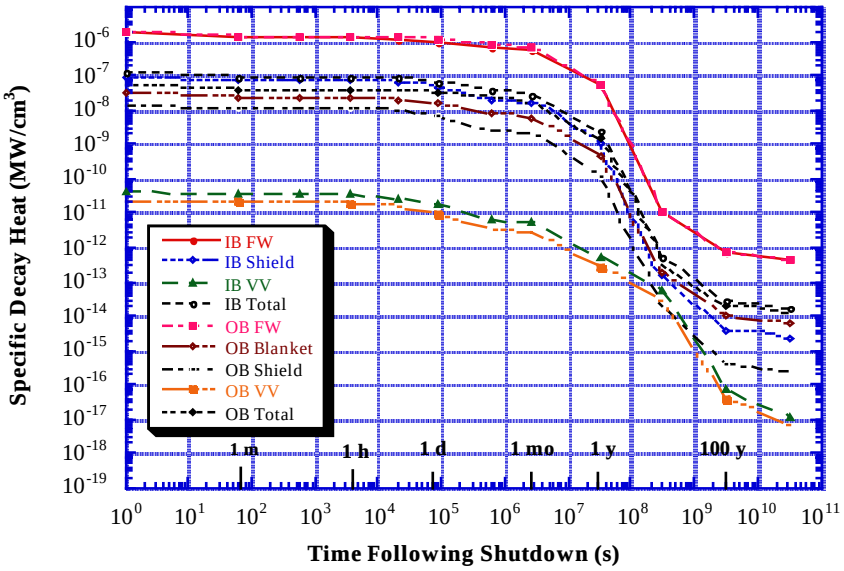

Fig. 10.4-2. Decay heat induced in the different components of EVOLVE as a function of time following shutdown.

Table 10.4-II. List of Dominant Nuclides.

	Activity	Decay Heat
Short-term < 1 day	^{185}W, ^{181}W ^{18}	^{4} Re, ^{185}W
Intermediate-term < 1 month	^{181}W, ^{185}W ^{1}	^{84} Re, ^{185}W
Long-term > 1 year	^{179} Ta, ^{186m} Re	^{182} Ta, ^{186m} Re

10.4.3 Waste Disposal Ratings

The radwaste of the different components of EVOLVE were evaluated according to both the NRC 10CFR61 and Fetter waste disposal concentration limits (WDL). The 10CFR61 regulations assume that the waste disposal site will be under administrative control for 100 years. The dose at the site to an inadvertent intruder after the 100 years is limited to less than 500 mrem/year. The waste disposal rating (WDR) is defined as the sum of the ratio of the concentration of a particular isotope to the maximum allowed concentration of that isotope taken over all isotopes and for a particular class. If the calculated WDR = 1 when Class A limits are used, the radwaste should qualify for Class

A segregated waste. The major hazard of this class of waste is to individuals who are responsible for handling it. Such waste is not considered to be a hazard following the loss of institutional control of the disposal site. If the WDR is > 1 when Class A WDL are used but = 1 when Class C limits are used, the waste is termed Class C intruder waste. It must be packaged and buried such that it will not pose a hazard to an inadvertent intruder after the 100 years institutional period is over. Class C waste is assumed to be stable for 500 years. Using Class C limits, a WDR > 1 implies that the radwaste does not qualify for shallow land burial.

Fetter developed a modified version of the NRC's intruder model to calculate waste disposal limits for a wider range of long-lived radionuclides which are of interest for fusion researchers than the few that currently exist in the current 10CFR61 regulations. Fetter's model included more accurate transfer coefficients and dose conversion factors. However, while the NRC model limits the whole body dose to 500 mrem or the dose to any single organ (one of seven body organs) to 1.5 rem, Fetter limits are based on the maximum dose to the whole body only.

Specific activities calculated by the DKR-PULSAR2.0 code were used to calculate the waste disposal ratings (WDR). The waste disposal ratings for the Fetter and 10CFR61 limits are shown in Tables 10.4-III and 10.4-IV, respectively. Results in the tables are given for compacted wastes. Compacted waste corresponds to crushing the solid waste before disposal (to eliminate voids in the structure) and thus disallowing artificial dilution of activity. The Class C WDR were calculated after a one-year cooling period. The dominant nuclides are given between brackets.

As shown in Table 10.4-III, according to Fetter limits, the first wall, blanket, and inboard shield would not qualify for disposal as Class C waste. As a matter of fact the W-5Re alloy produce such a high activity that the first wall would have a WDR which is more than order of magnitude higher than the Class C WDR limits. The high WDR is due to the ^{186m}Re, ^{108m}Ag, and ^{94}Nb isotopes. Only ^{186m}Re is a product of nuclear interactions with base elements in the W-5Re alloy. On the other hand, ^{108m}Ag($T_{1/2}$ = 130 yr), and ^{94}Nb($T_{1/2}$ = 20,000 yr) are produced by nuclear interactions with the niobium and silver impurities present in the W-5Re alloy used in the analysis. All of the other components would qualify for disposal as Class C waste. Results in Table 10.4-VI show that according to the 10CFR61 limits, the first wall and blanket would not qualify for disposal as Class C waste. The waste disposal ratings of all components are dominated by contribution from the ^{94}Nb isotope.

Since the first wall and secondary blanket will not meet the limits for Class C disposal, we examined the impact of producing non-low level waste on the total volume of waste generated. The first wall has a life-time of 5 FPY and the secondary blanket is a life-time component. The first wall represents less than 3% of the total volume of the waste (excluding magnets). Replacing the first wall every 5 years means that about 15% of the total volume of the waste (excluding magnets) would not qualify for shallow land burial as low level waste. On the other hand, with the secondary blanket we have a choice of either replacing it every ~ 2 FPY and hence allowing for its disposal as Class C LLW,

or keeping it for 30 FPY and disposing it as non-low level waste. Since the secondary blanket represents less than 3% of the total volume of the waste (excluding magnets), replacing it every 2 FPY would increase the total volume of the LLW by about 40%.

In conclusion, in EVOLVE we have the choice between generating less than 20% of the waste volume (excluding magnets) as non-low level waste or limiting the non-low level waste to about 10% while increasing the total waste volume (excluding magnets) by about 40%. Finally, adding the volume of the magnets to the total volume of the waste generated will results in a significant reduction in percentage contribution of the non-low level waste to the total volume of waste generated.

Table 10.4-III. Class C Waste Disposal Ratings Using Fetter Limits.

Zone	FPY	WDR	Dominant Nuclides
Inboard FW	***5***	***19.9***	^{108m}Ag, ^{186m}Re, ^{94}Nb
Inboard Shield	***30***	***1.5***	^{94}Nb, ^{108m}Ag, ^{186m}Re
Inboard VV	***30***	***0.015***	^{94}Nb
Outboard FW	***5***	***20.8***	^{108m}Ag, ^{94}Nb, ^{186m}Re
Outboard Blanket	***30***	***17.6***	^{94}Nb, ^{108m}Ag, ^{186m}Re
Outboard Shield	***30***	***0.226***	^{94}Nb
Outboard VV	***30***	7.86×10^{-3}	^{94}Nb

Table 10.4-IV. Class C Waste Disposal Ratings Using 10CFR61 Limits.

Zone	FPY	WDR	Dominant Nuclides
Inboard FW	***5***	***4.24***	^{94}Nb
Inboard Shield	***30***	***0.896***	^{94}Nb
Inboard VV	***30***	***0.016***	^{94}Nb
Outboard FW	***5***	***3.54***	^{94}Nb
Outboard Blanket	***30***	***6.97***	^{94}Nb
Outboard Shield	***30***	***0.165***	^{94}Nb
Outboard VV	***30***	8.46×10^{-3}	^{94}Nb

10.5 Power Conversion

The schematic of the power conversion system is shown in Fig. 10.5-1There are two coolant streams exiting from the blanket. The front part of the blanket, including the first wall, is cooled by boiling lithium, which carries ~2/3 of the total thermal power. The lithium vapor exits from the blanket at 1200 ^{o}C and 0.35 bar pressure. The back part of the blanket is cooled by a conventional self-cooled liquid lithium blanket with an exit temperature of also 1200 ^{o}C, which carries the other 1/3 of the thermal power.. The reason that a second breeding zone is necessary is to increase the lithium density for tritium breeding considerations.

The two blanket coolant streams will be fed to two heat exchangers to transfer the thermal energy to a helium loop. The reason that He is used for the secondary coolant is that a closed cycle gas turbine can be used for very efficient power conversion. The two lithium streams exit from the blanket operates in series, with the liquid lithium stream to heat up the secondary He from 700 to 800 ^{o}C, while the high temperature lithium vapor super heat the same He stream from 800 to 1000 ^{o}C. The He at 1000 ^{o}C will enter a He turbine for power conversion.

The parameters of the power conversion system are summarized on Table 10.5-1. With a very high He temperature, and very high recuperator, compressor and turbine efficiencies, a very high cycle efficiency of 57.7% is calculated. This thermal efficiency

includes the pumping power of the secondary He stream, but does not include the pumping power of either of the lithium streams.

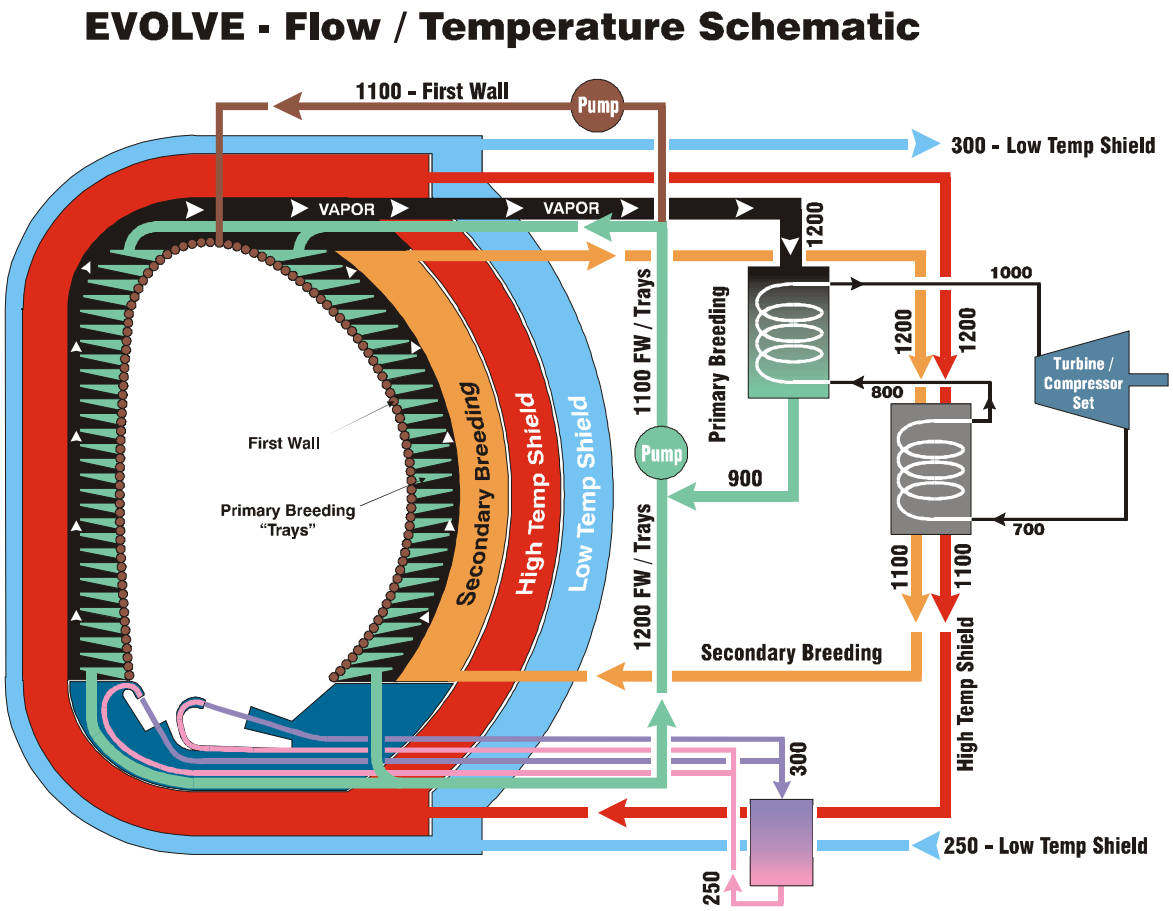

Fig. 10.5-1. Flow/temperature schematic for EVOLVE concept

Table 10.5-1. Power Conversion Parameters for the EVOLVE Concept

Parameter	Name	Value
To, K	Turbine inlet temperature	1273
Ts, K	Compressor inlet temperature	308
To/Ts		4.13
r	Compression ratio	2.0
nx	Recuperator efficiency	0.96
nc	Compressor efficiency	0.92
nt	Turbine efficiency	0.92
Beta	Turbine pressure ratio	1.02
Gamma	Gas heat capacity ratio (Cp/Cv)	1.66
Cycle efficiency		57.7%

10.6 Thermo-mechanical Analysis

This section summarizes the thermal and stress analyses for the lithium spray cooled EVOLVE first wall subjected to surface heat fluxes of 1.5 and 2 MW/m^2, a coolant temperature of 1200°C, and a coolant pressure of 0.05 MPa. A single tungsten tube of radius 2.5 cm and wall thickness of 3 mm deforming under generalized plane strain condition is considered. For the heat conduction analysis, a sinusoidal heat flux profile on the first wall is assumed, as shown in Fig. 10.6-1.

Design allowables for tungsten

The allowable stresses for tungsten applicable for elastic analysis design rules are derived using the procedures given in Chapter 13.2.

Time-independent allowable

The variation of S_m with temperature for annealed tungsten is shown in Fig. 2a. Note that the value of S_m at = 1200°C is constant at 30 MPa up to 1900°C and is > 20 MPa at 2000°C.

Time-dependent allowable

The time-dependent primary membrane stress intensity allowable S_{mt} is defined as

$$S_{mt} = \text{Min}\ (S_m, S_t) \qquad (2)$$

where S_t, which is a function of both time and temperature, is defined in Chapter 13.2. However, since only the creep rupture time data for tungsten were available, the allowable stress intensity is denoted by S_{rt}. Variation of S_{rt} with time and temperature is given in Fig. 2b. Note that as long as the average first wall temperature is less than 1400°C, S_m determines the value of S_{mt}.

The primary membrane stress in the EVOLVE first wall is so low that neither low-temperature nor high-temperature ratcheting should be a limiting criterion for the surface heat flux. The peak surface heat flux will be controlled either by creep-fatigue (which is not considered here) or possibly by brittle fracture (due to helium-embrittlement). Because of lack of data, we will consider a conservative limiting case of zero ductility.

Primary stress

The primary membrane stress due to the coolant pressure is only 0.33 MPa. A comparison with Figs 10.6-2a-b shows that this stress is too low to be of concern.

Secondary stress

Heat conduction and thermal stress analyses were conducted for three cases, all with a coolant temperature of 1200°C. In the first case, a peak surface heat flux of 1.5 MW/m^2 was analyzed with an assumed solid to coolant heat transfer coefficient of 10,000 W/m^2/°C. In the second case, a peak surface heat flux of 2 MW/m^2 was

analyzed for an assumed solid to coolant heat transfer coefficient of 40,000 W/m^2/°C and finally, in the third case the same problem was analyzed for an infinite heat transfer coefficient. It is expected that the third case closely approximates the lithium spray cooling condition of the first wall that is envisioned for EVOLVE.

Case 1 (1.5 MW/m^2)

The temperature distribution in the first wall for a surface heat flux of 1.5 MW/m^2 and a coolant heat transfer coefficient of 10,000 W/m^2/°C is shown in Fig. 10.6-3. The plasma side peak temperature is 1404°C. Note that a maximum through-thickness temperature drop of ~ 50°C occurs at the top of the tube is and a significant fraction of the heat is conducted circumferentially to the colder part of the tube in the back. The distribution of the stress intensity (Fig. 10.6-4) shows that a maximum 237 MPa occurs at the location of the peak temperature. An inspection of Fig. 10.6-2a shows that this stress exceeds the $3S_m$ limit at the cross section-averaged temperature of 1250°C. However, it would be extremely conservative to apply the $3S_m$ rule to a case where the primary stress is so low. An application of either the low temperature or the high temperature ratcheting rule (Chapter 13.2) shows that either ratcheting limit is easily satisfied for this low pressure and 1.5 MW/m^2 surface heat flux.

Case 2 (2 MW/m^2, h=40,00 W/m^2/°C)

The temperature distribution for this case (Fig. 10.6-5) shows a peak temperature of 1317°C with most of the heat conduction at the peak temperature location occurring radially . The peak stress intensity (Fig. 10.6-6) is 158 MPa, which as in Case 1 easily satisfies the ratcheting limits.

Case 3 (2 MW/m^2, h=∞)

The temperature distribution for this case (Fig. 10.6-7) shows a peak temperature of 1261°C with very little heat conduction along the circumference. The peak stress intensity (Fig. 10.6-8) is only 99 MPa, which as in Case 1 easily satisfies the ratcheting limits.

Embrittlement issue

Until now we have assumed that tungsten does not undergo embrittlement either due to irradiation or helium embrittlement. No relevant data are currently available. If we assume conservatively that either the uniform elongation is < 2% or the ductility (i.e., %Reduction in Area) of tungsten is reduced to zero, then the S_d limit (stress limit with embrittlement) for this material at 1200°C is 150 MPa. Although this will reduce the maximum surface flux limit for case 1, for the more realistic case (Case 3) of very high heat transfer coefficient, the peak stress due to 2 MW/m^2 would be within the S_d limit. It

would exceed the S_d limit slightly for the smaller heat transfer coefficient of 40,000 $W/m^2/°C$. However, it should be noted that very little ductility is needed to raise the S_d limit to a high value. For example, if the uniform elongation remains higher than 2%, the S_d value corresponding to a ductility of %RA=1, is raised to > 300 MPa.

Conclusions

If the primary stresses are extremely low and the heat transfer coefficient at the solid to coolant interface is very high (as would be expected for lithium spray cooling), a surface heat flux of 2 MW/m^2 can be tolerated by the EVOLVE tubular design. Even if the ductility of tungsten is reduced to zero, the thermal stresses are sufficiently low so that the peak stress satisfies the S_d limit.

The maximum surface heat flux capability of the EVOLVE tubular first wall will be set by either creep-fatigue or reduced fracture toughness (K_{IC}) due to the irradiation environment.

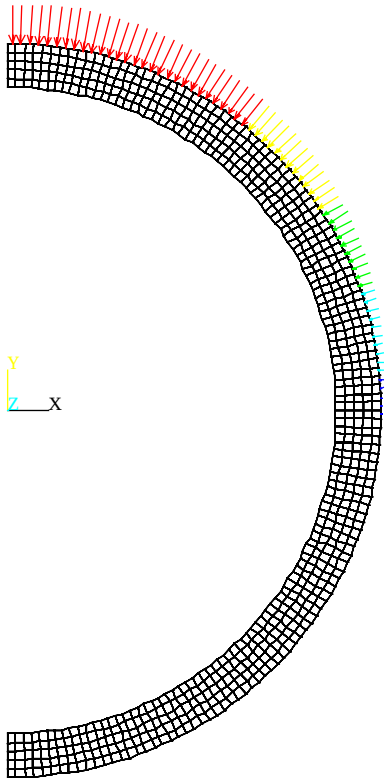

Fig. 10.6-1 Assumed sinusoidal surface heat flux distribution on first wall. Plasma is at top.

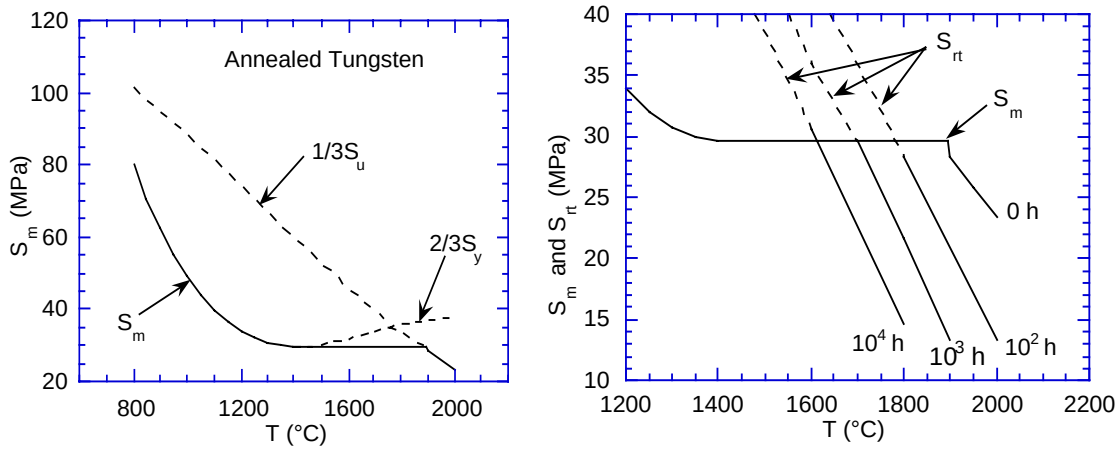

(a) (b)

Fig. 10.6- 2 (a) Time-independent primary membrane stress intensity allowable S_m and (b) time-dependent primary membrane stress intensity allowable S_{rt} for annealed tungsten.

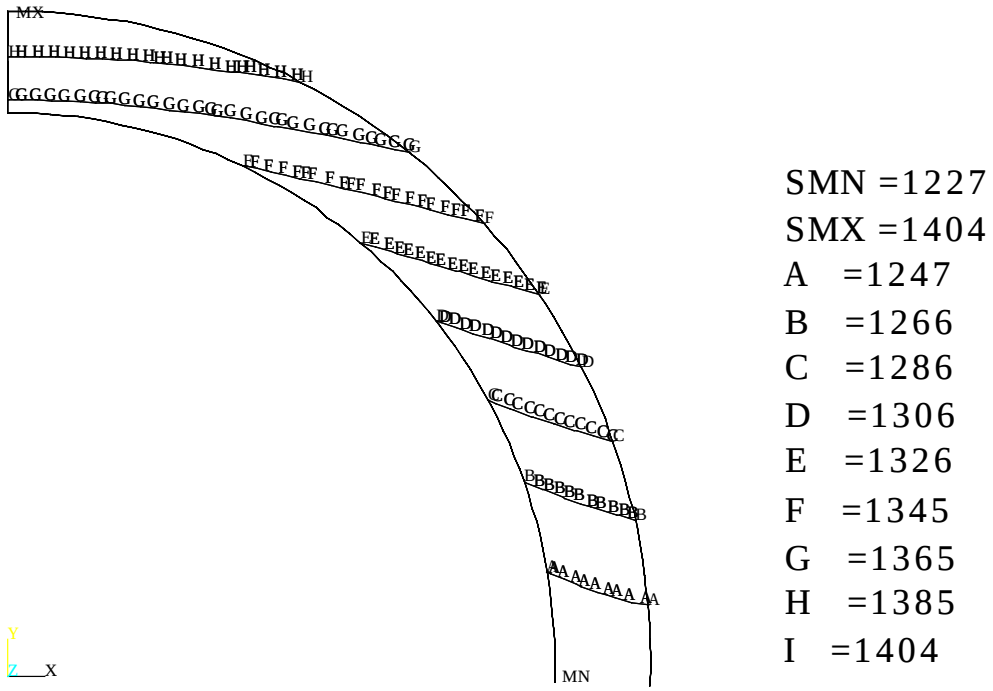

Fig.10.6-3 Temperature distribution in W first wall due to a peak surface heat flux of 1.5 MW/m^2, coolant temperature of 1200°C and coolant-first wall heat transfer coefficient of 10^4 W/m^2/°C (Case 1).

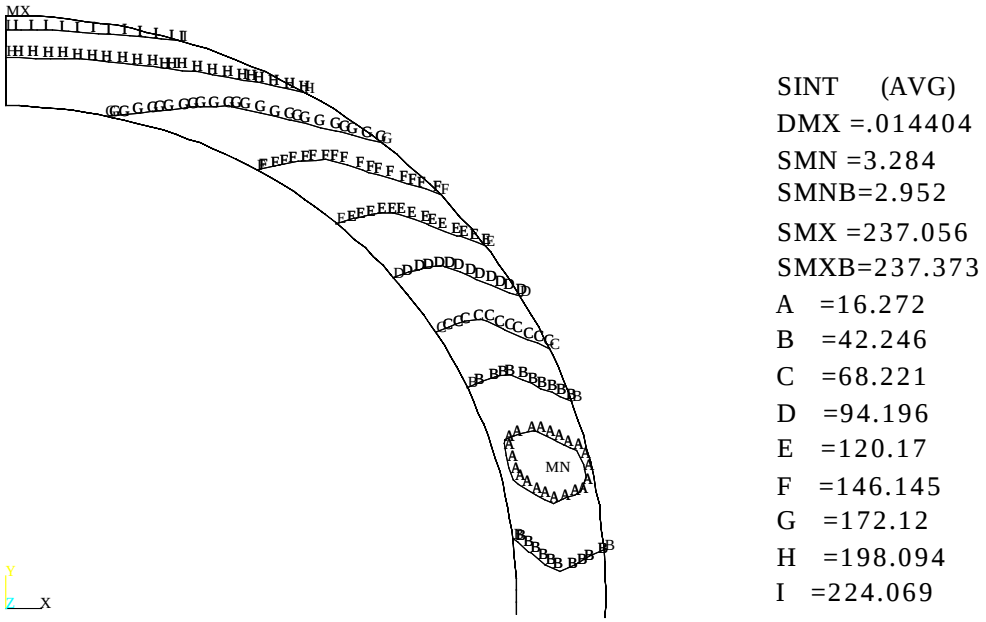

Fig. 10.6-4 Distribution of stress intensity (MPa) due to the temperature profile of Fig. 10.6-3 and a coolant pressure of 0.05 MPa (Case 1).

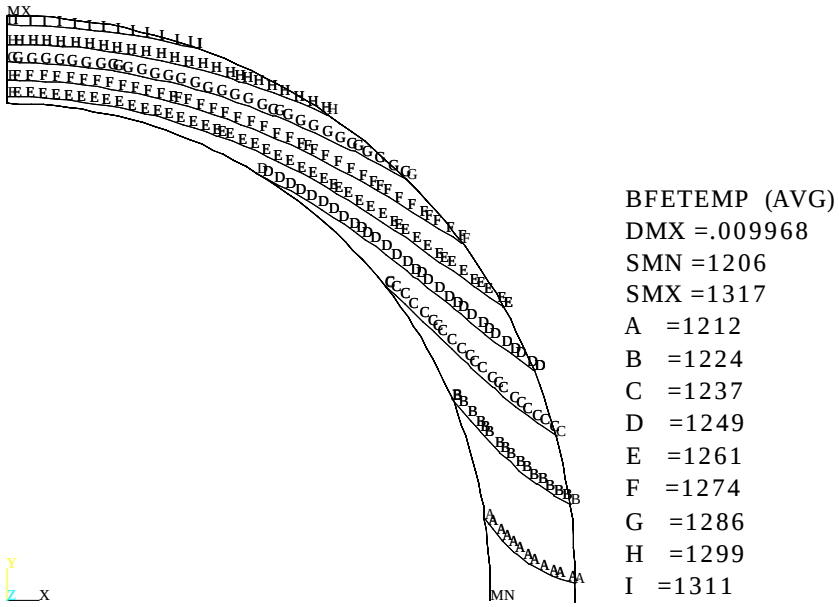

Fig. 10.6-5 Temperature distribution in W first wall due to a peak surface heat flux of 2 MW/m^2, coolant temperature of 1200°C and coolant-first wall heat transfer coefficient of 4x10^4 W/m^2/°C (Case 2).

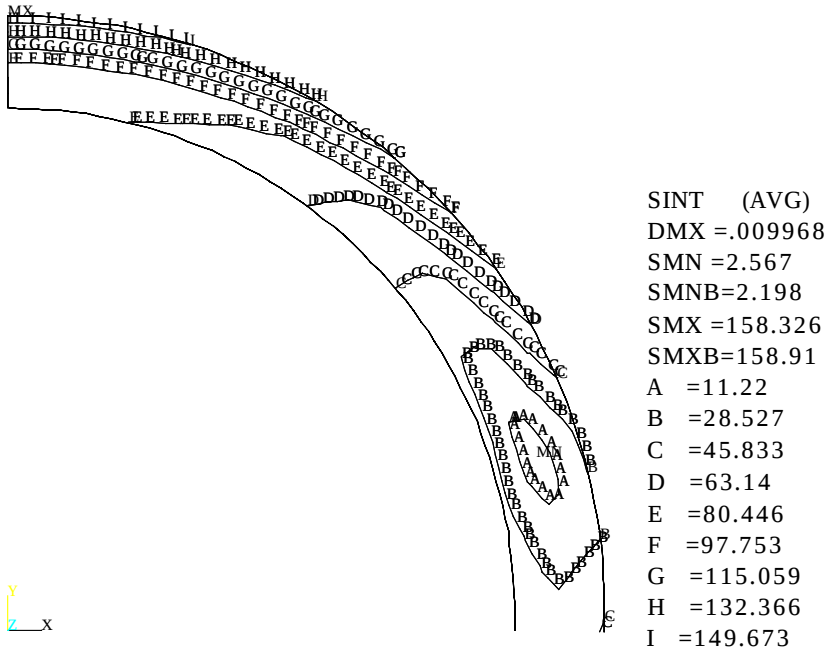

Fig. 10.6-6 Distribution of stress intensity (MPa) due to the temperature profile of Fig. 10.6-5 and a coolant pressure of 0.05 MPa (Case 2).

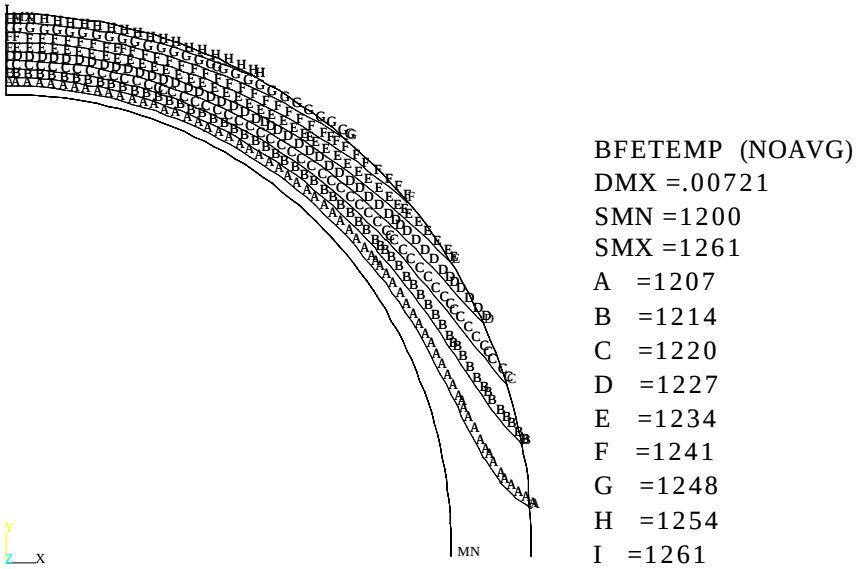

Fig. 10.6-7 Temperature distribution in W first wall due to a peak surface heat flux of 2 MW/m^2, coolant temperature of 1200°C and coolant-first wall heat transfer coefficient of infinity (Case 3).

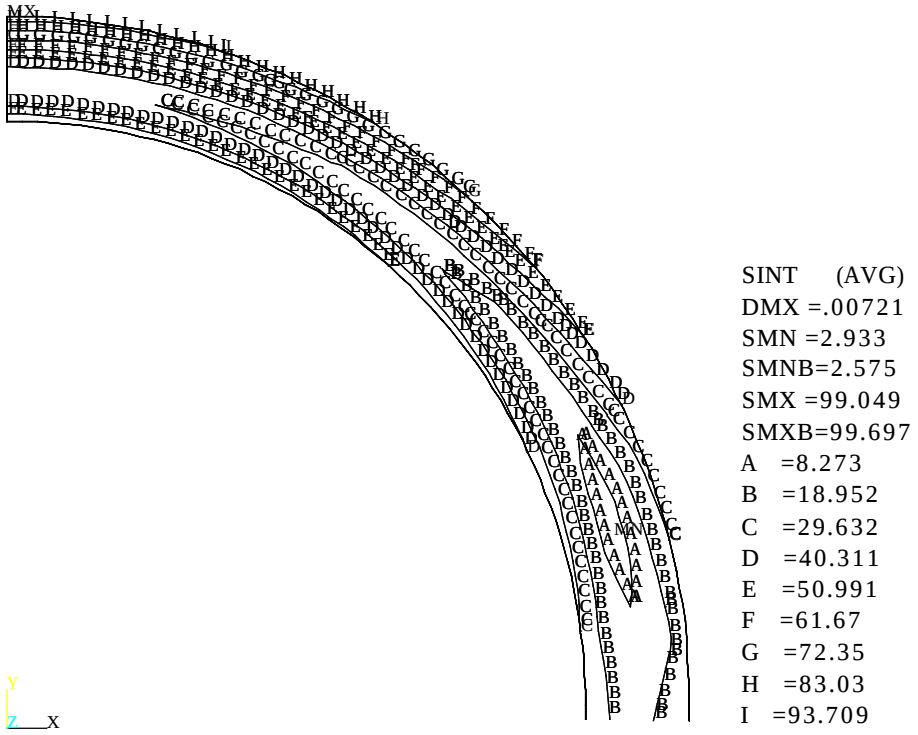

Fig. 10.6-8 Distribution of stress intensity due to the temperature profile of Fig. 10.6-7 and a coolant pressure of 0.05 MPa (Case 3).

10.7 Tritium extraction

The tritium solubility in lithium is very high. Therefore, the tritium vapor pressure over lithium is very low, with a reasonable tritium concentration in the lithium. The typical design goal for tritium recovery system is to limit the tritium concentration in the lithium to about 1 appm. At this concentration, the tritium inventory in the breeding is about 200g, while the tritium partial pressure over lithium is 10^{-7} Pa at 600 ^{o}C. With the low tritium partial pressure and reasonable tritium concentration, the tritium recovery process will recover tritium from the liquid phase.

A new tritium recovery process from liquid lithium has been proposed under ITER activities[1]. This method is based on cold trapping. Cold trapping demonstrated for tritium recovery to the solubility limit, which is ~250 appm at 200 ^{o}C. The proposal here is to add protium in the lithium so that the tritium concentration can be reduced to 1 appm, while the total hydrogen concentration is about the saturation limit. The attractive feature of this process is that no impurities will be added into the lithium. The cost is that protium will be added, that tritium has to be separated from protium.

With Li(T+H) super saturated in the cold trap, it will precipitate out. There is a large difference in density between lithium (0.5) and LiH (0.8). therefore LiH can be separated from lithium by gravitational force. (A process called meshless cold trap was developed for the breeder program based on the same principle)[2]. The Li(H+T) can than be heated up to 600 ^{o}C, at this temperature Li(H+T) will be decomposed to Li and (H+T). The Decomposed product of Li and (H+T)will be passed over cold trap of 200 ^{o}C, in which Li will be condensed. The (H+T) will pass a permeation window to assure the purity of the hydrogen stream, before it is fed to the Isotope Separation System (ISS) to separate H from T.

A detailed calculation for the design of the ITER ISS was performed based on the reference ITER parameters, with the addition of the (H+T) stream with H/T ratio of 1000. The additional cost associated with the separate the H/T from the blanket tritium recovery system, as well as the additional refrigeration power required, are rather modest[3].

10.8 Safety

As shown in Section 10.4, the level of afterheat with tungsten is relatively high, and suitable means for removing the afterheat need to be identified. The flow paths for the coolant have been designed such that a passive flow will allow flow afterheat removal, as shown in Fig. 10.8-1. Further analysis of afterheat removal is planned for the future.

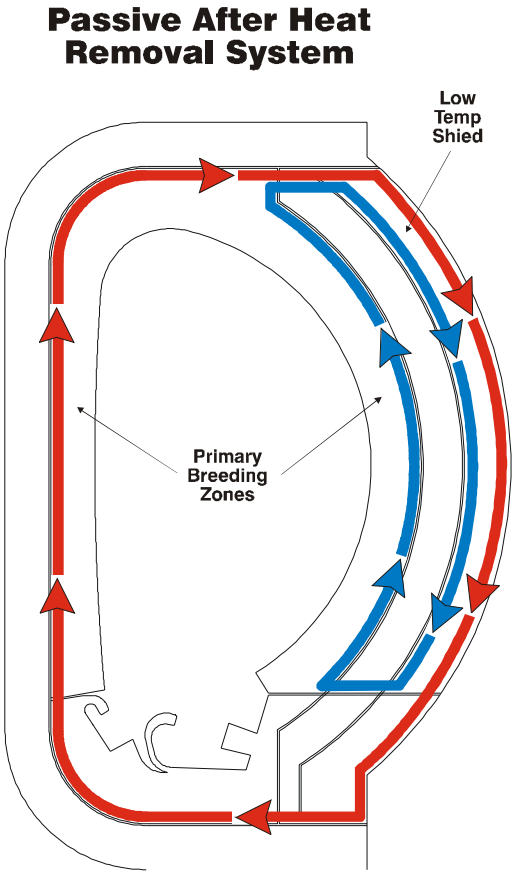

Figure 10.8-1 Flow path for passive removal of afterheat.

10.9 Critical issues, required R&D

It has been already mentioned that the work on the EVOLVE concept is at a very early stage. The main emphasis in the program is to assess the potential of the concept, identify crucial issues which may became feasibility issues, and to define most needed R&D work to remove the important question marks. No detailed design work, comprehensive analyses, or concept optimization is required at this stage. In this spirit, the following main questions should be addressed :

1 Will the backside of the first wall remain wetted under all conditions?

The liquid metal is supplied to the heated surface by an array of jets. Vapor will be generated in the liquid metal film and has to escape from the surface. Surface tension has to keep the wall wetted. This is the same principle as successfully employed in heat pipes where in addition the liquid metal has to be transported over a relatively large distance by capillary forces. This "pumping" is in heat pipes facilitated by grooves, porous walls or a suitable wick structure. The conditions with actively pumped arrays of jets are probably even more favorable for high heat flux removal but the required surface conditions and the heat flux limits of the EVOLVE concept will have to be investigated.

2 *Will the vapor generated in the stagnant boiling pools of the primary breeding region separate fast enough ftom the liquid metal?*

The trays in the breeding zone contain a lithium pool with a height of 10 to 20 cm. The bottom of this pool is made of tungsten with about 5 mm thickness. The peak volumetric heat generation in the tungsten structure is about 100 W/cm^3, in the lithium pool about 10 W/cm3. This results in a rather high rate of lithium vapor generation. The important question is, how the vapor will rise inside the pool to the surface and how it will separate there from the liquid metal. If this boiling process is similar to boiling water, the liquid metal density will remain reasonably high. However, if the lithium boils like milk, the liquid metal density could become too low for sufficient tritium breeding and shielding. The problem becomes even more complicated by the presence of the strong magnetic field, damping all fast liquid metal movements.

It has been suggested, that under these conditions discrete sites for initiating bubbles at the bottom of the tray should be triggered in order to generate a desired pattern of vapor flow channels with increasing diameters from the bottom to the surface. This mechanism is supported by the larger heat generation in the tungsten bottom plate. No liquid metal movement would be necessary for this pattern since the vapor channels are stationary. This model, however, is an assumption at the moment and suitable modeling and possible experiments are required to prove the feasibility of the vapor separation.

3 Will the liquid metal overflow system work and lead to equal liquid metal pressure in each tray?

The stack of trays in each blanket segment is about 3 m high. There is a supply tube located at the top tray and a drain tube at the bottom tray to extract excess liquid metal. The trays are all connected with standpipes (similar to the ones commonly used in showers) which maintain a constant level in each tray and supply the liquid metal to the tray below. The trays are connected directly in vertical direction by the vapor manifolds only. This arrangement should result in equal liquid metal height and pressure in every tray, provided the MHD pressure drops in the standpipes can be overcome by small static heads. Using thin-walled inserts in the standpipes can reduce the MHD pressure drop but it should be investigated if this is sufficient or if MHD flow coupling has to be employed to insure the desired liquid metal flow.

4 Is it possible to fabricate entire blanket segments of tungsten or tungsten- alloys in spite of their low ductility and their limited weldability?

The EVOLVE FW/blanket design allows for large fabrication tolerances and has minimum requirements on the strength of welds. Most of the welds would not even need to be leak proof. Primary and secondary stresses in the blanket structure are minimized by the design. But nevertheless, the feasibility of fabricating these segments with such a material has to be investigated. It has been suggested to facilitate the fabrication by using

a combination of tungsten and tantalum alloys but again this possibility would have to be investigated.

5 How will the structural material behave under intense neutron irradiation?

There is very little experience with tungsten under neutron irradiation. The general trend is that the material becomes even more brittle already at low fluence. However, all the irradiation experiments had been performed at relatively low temperatures < 700 C and they are not relevant for temperatures > 800 C as envisaged in the entire EVOLVE blanket structure. Neutronics calculations show that the dpa-rates and the helium generation rate in tungsten are much lower than in steel or vanadium but which values are allowable with this material? Some estimates at least based on suitable models about these issues are required.

6 Will the high after heat in tungsten cause a safety problem in case of a LOCA ?

The after heat in tungsten at shutdown amounts to about 2 % of the full power value and is considerably higher than the one in steel. Without any cooling in case of a LOCA , temperatures > 1500 C could be reached for longer periods of time. These estimates are, however, based on over-conservative assumptions for the following reasons :

a) The front zone including FW and primary breeding zone is cooled by a loop separated from the cooling loop for secondary breeding zone/shield. If one of the two systems remain operational, the maximum tungsten temperature will probably fall much below 1500 C.
b) The FW/blankets in each torus sector have their individual cooling system. The after heat in the failed sector can be radiated at relatively low temperatures to the other sectors.
c) If the cooling of the vacuum vessel remains operational, the EVOLVE FW/blanket can probably radiate away the afterheat to the vacuum vessel at maximum temperatures below 1500 C.

More analyses are required to find out if there is a significant safety problem caused by a LOCA in the EVOLVE system.

References:

1. D. K. Sze, R. F. Mattas, J. Anderson, R. Haange, H. Yoshida, O. Kveton, Tritium Recovery from Lithium Based on Cold Trap, ISFNT-3, Los Angles, June 1994
2. R. L. Eichelberger, Testing of a Meshless Cold Trap for Hydrogen Removal from Sodium, Proceeding of the Second International Conference on Liquid Metal Technology in Energy Production." Richland Washington, April 20-24, 1980
3. O. Kveton, ITER JCT Naka, Personal communication